REPUBLIC OF TURKEY

ACIBADEM MEHMET ALİ AYDINLAR UNIVERSITY
INSTITUTE OF NATURAL AND APPLIED SCIENCES

DEVELOPMENT OF DUAL-FUNCTIONAL BIOACTIVE HYDROGELS FOR NERVE TISSUE DAMAGE

İLEYNA SEVDE ÜVAK

MASTER THESIS

BIOMEDICAL ENGINEERING PROGRAMME

SUPERVISOR

Assist. Prof. Özgül GÖK

ISTANBUL – 2021

Tez Onay Sayfası

DECLARATION

I declare that this thesis has been composed by myself and it has not been submitted in any previous application for any other degree. Except for collaborative contributions, the experimental work and the data analysis were entirely done on my own. References have been used for supporting literature.

ACKNOWLEDGMENT

First, I would like to thank my advisor, Assist. Prof. Özgül Gök for her guidance, great support, patience, and encouragement throughout my research studies. Her confidence in me made me more productive. She also taught me how to handle stress and tough times in academia.

I would like to extend my thanks to my committee Prof. Fatma Neşe Kök and Assoc. Prof. Özge Can for their careful and constructive review of the final manuscript. Also, I would like to thank current members and alumni of Gök Lab. A team that whenever I needed help or had some questions was there to answer. Besides, thank you to those not specifically mentioned who I also consider my friend or help along the way.

I like to express my sincere gratitude and love to my family. I am very grateful to my mother (Pınar Üvak) and my father (Abdurrahman Üvak) for supporting me and my education no matter what, and my brother (İbrahim Enes Üvak). I could not be more grateful for what they have taught me and made me who I am.

Finally, I owe Çağatay İleri my deepest thanks for his unconditional and continuous love, support, patience, guidance, motivation, and trust. He has stood by me through all my travails, my absences, and my impatience.

This project was financially supported by TUBITAK 1002 program with Project No: 119Z637.

TABLE OF CONTENT

LIST OF ABBREVIATION

APS	Ammonium persulfate
CNS	Central Nervous System
DI	Distilled Water
DMAP	4-Dimethylaminopyridine
DMF	N, N-Dimethylformamide
DMPA	Dimethoxy-2-phenylacetophenone
DMSO	Dimethyl Sulfoxide
ECM	Extra Cellular Matrix
EDS	Energy Dispersive X-Ray Spectroscopy
Et_3N	Triethylamine
FT-IR	Fourier Transform-Near Infrared Spectroscopy
HA	Hyaluronic Acid
HA-MA	Hyaluronic Acid- Methacrylate
HCl	Hydrochloric Acid
HNMR	Proton Nuclear Magnetic Resonance
MA	Methacrylate
MAC	Methacryloyl Chloride
NaOH	Sodium Hydroxide
NH_2-HCl	2-Aminoethyl Methacrylate Hydrochloride
PBS	Phosphate Buffered Saline
PEGdiMA	Poly (ethylene glycol) Dimethacrylate
PNS	Peripheral Nervous System
SEM	Scanning Electron Microscopy
TBA-F	Tetrabutylammonium Fluoride
TEMED	Tetramethyl Ethylenediamine

LIST OF FIGURES

LIST OF TABLES

SUMMARY

The synthesis and characterization of bioactive hydrogels were successfully synthesized within the scope of this research project. These hydrogels are biomaterials which utilized as porous three-dimensional scaffolds. Integrated versions of diverse biomolecules are being developed to expand their application as artificial tissues in soft tissue engineering. The goal of this project is to create a method for derivatizing hyaluronic acid (HA) with polymerizable methacrylate residues, a functionalized short laminin peptide attachment, and an anti-inflammatory drug loading to create a bioactive hydrogel with precise control for neural tissue damage therapy. Methacrylate groups were successfully attached to HA, in two procedures. Via methacrylic anhydride and methacryloyl chloride. Methacrylic anhydride was chosen due to efficiency and efficacy. It was also possible to encapsulate drug molecules into hydrogel scaffolds for anti-inflammatory effects. Attachment of the peptide sequence covalently that contains free thiol group in its structure can increase cell adhesion to polymeric surfaces which this hydrogel scaffold provides. This reaction between the maleimide molecule, and the peptide molecule, which also has free SH group at one end, was carried out with the help of a photo initiator and under UV light (365 nm). After the optimization steps, the hydrogel structure with the most suitable properties was selected. Within the purpose, the gelation rates of two different photo initiators were examined and it is expected that the derivatized HA hydrogel structure encapsulating drug and peptide molecules will be suitable for both neural cell adhesion and proliferation.

Keywords: Hyaluronic Acid, Methacrylate, Peptide conjugate, Nerve regeneration, Hydrogels

ÖZET

Sinir Doku Hasari İçin Çift Fonksiyonlu Bioaktif Hidrojellerin Geliştirilmesi

Bu araştırma projesi kapsamında biyoaktif hidrojellerin sentezi ve karakterizasyonu başarıyla tamamlanmıştır. Bu hidrojeller, gözenekli üç boyutlu yapı iskeleleri olarak kullanılan biyomalzemelerdir. Yumuşak doku mühendisliğinde bir yapay doku parçası olarak uygulamalarını genişletmek için çeşitli biyomoleküllerin entegre versiyonları geliştirilmektedir. Bu projenin amacı, nöral doku hasarı tedavisi için kesin kontrole sahip biyoaktif bir hidrojel oluşturmak için polimerize edilebilir metakrilat kalıntıları, işlevselleştirilmiş kısa laminin peptit eki ve anti-inflamatuar ilaç yüklemesi ile hyaluronik asidi (HA) türevlendirmek için bir yöntem oluşturmaktır. HA'ya metakrilat gruplarının bağlanması metakrilik anhidrit ve metakriloil klorür yoluyla iki prosedürde başarılı oldu. Verimlilik ve etkinlik nedeniyle metakrilik anhidrit seçildi. İlaç moleküllerini, anti-inflamatuar etkiler için hidrojel iskelelerine kapsüllemek ve yapısında serbest tiyol grubu içeren ve bu hidrojel iskelesinin sağladığı polimerik yüzeylere hücre yapışmasını artırabilen peptit sekansını kovalent olarak bağlamak da mümkün olmuştur. Maleimid molekülü ile bir ucunda serbest SH grubu bulunan peptit molekülü arasındaki bu reaksiyon, bir foto başlatıcı yardımıyla ve UV ışığı (365 nm) altında gerçekleştirilmiştir. Optimizasyon adımlarından sonra en uygun özelliklere sahip hidrojel yapısı seçilmiştir. Proje kapsamında iki farklı fotobaşlatıcının jelleşme hızları incelenmiş olup, Hyaluronik asit türevli polimeri içine alan hidrojel yapısının hem nöral hücre adezyonu hem de proliferasyonu için uygun olması beklenmektedir.

Anahtar sözcükler: Hyaluronik Asit, Metakrilat, Peptid konjugatı, Sinir rejenerasyonu, Hidrojeller

1. BACKGROUND AND AIM OF THIS STUDY

This project aims to develop a method to derivatize hyaluronic acid (HA) with polymerizable methacrylate residues with a functionalized short laminin peptide attachment and an anti-inflammatory drug loading which results in a bioactive hydrogel with precise control for neural tissue damage therapy. This bioactive hydrogel aims to enhance neural cell survival and promote axonal outgrowth and neural regeneration with hyaluronic acid residues and added short laminin peptide with the addition of anti-inflammatory drug. The bioactive hydrogel is expected to mimic the native physiological environment of healthy neural tissues and regulate cell behavior and support the regenerate injured nerve tissues.

Within the scope of the project, it is achieved to prepare biocompatible hydrogels that may act selectively on target cells and to provide slow and controlled release of drug molecules to be applied in treatment. Later, these hydrogels were printed in a certain manner presumably will help the nerve cells to grow and repair the damaged areas. This allows for the combined use of targeted drug delivery and three-dimensional scaffold structures for both local applications of biomaterials and delivery of therapeutic agents in a controlled and sustained manner specified in the targeted (and mostly exposed to inflammation) neural cells.

2. INTRODUCTION

2.1. Tissue Engineering

Tissue engineering is an interdisciplinary field that constructs tissue-like structures by integrating cells, biomaterials, biochemical (i.e., growth factors), and physical (i.e., mechanical loading) signals. Tissue engineering focuses on creating biological replacements that can support damaged tissues' preservation, repair, or increase the damaged tissues' function (1).

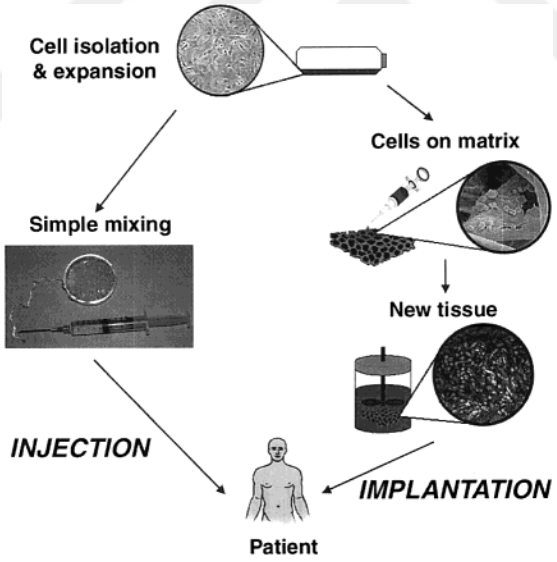

Figure 2.1. Schematic illustrations of tissue engineering applications (2).

The desire to repair damaged tissues has resulted in the clinical necessity for tissue engineering and regenerative medicine. Traditional methods are not yet capable of completely or efficiently repairing such defects, regardless of how they occurred (acute or chronic). Traditional medicine has significant limitations in providing solutions to a wide range of health issues (3).

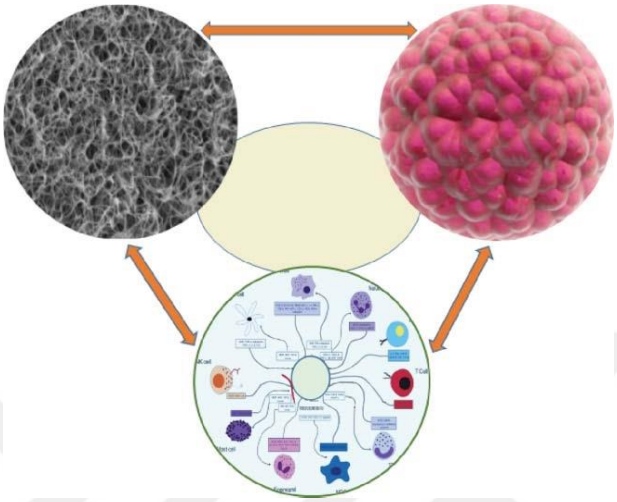

Figure 2.2. Schematic illustrations of tissue engineering applications (2).

While already-used medications can help with a variety of diseases, they cannot cure several lethal diseases (i.e., several types of cancer, strokes, diabetes) or diseases with neural system degeneration (i.e., Alzheimer's, Parkinson's).

Thus, the need to improve the methods of treatment increases, and tissue engineering is a relatively new area focusing on how to improve patient's lives. The ultimate objective is to overcome the necessity for organ transplantation one day by tissue engineering. In the organ waiting list, which is always continuing to rise at a greater speed than the number of organ donors, the medical needs for tissue engineering are emphasized.

2.1.1. Nerve tissue engineering

The two main components of the nerve system are the central and peripheral nervous systems (known as CNS and PNS). The CNS includes the brain and spinal cord, where PNS consists of the motor and sensory neurons to transmit stimuli signals from and to the CNS and enable interaction between the CNS and the whole body. The nervous system is vulnerable to damage that surpasses its inherent capacity to heal or regenerate due to its complex nature and specificity. Damage in the nervous system can be as demyelination of the nerves, total nerve degeneration, wound formation, or stimuli gap between neurons and support cells. Nerve tissue engineering is an interdisciplinary area where medicine and engineering combine to enhance nerve regeneration methods for patients who suffer from neural damage.

Different techniques are used with clinical methods to repair nerve tissue damages and promote nerve regeneration. These techniques include the usage of support cells such as stem cell therapy, growth factors, and biological and synthetic biomaterials. Biomaterials are utilized on damaged areas are called scaffolds. The scaffold design is detrimental in neural regeneration because the used scaffold should mimic the microenvironment of the extracellular matrix (ECM) and promote attachment, proliferation, growth, migration, differentiation, and survival of the cells (5).

2.2. Scaffolds Used in Nerve Tissue Engineering Applications

2.2.1. Natural, synthetic, and hybrid scaffolds

The scaffold design is crucial in neural regeneration because the scaffold should mimic the microenvironment of the extracellular matrix (ECM) and promote attachment, proliferation, growth, migration, differentiation, and survival of the cells (1).

Various nerve regeneration strategies use natural polymers scaffolds such as chitosan, chitin, collagen, gelatin, and alginate, synthetic non-degradable polymer scaffolds from polymers such as silicone, synthetic biodegradable polymers such as, polycaprolactone (PCL), poly L-lactic acid (PLLA), and conducting polymers such as polypyrene and polyaniline (6). Although these biomaterials are promising about fulfilling some stated criteria for scaffold properties, they have some disadvantages that needs to overcome to meet the specific tissue engineering applications. For example, a scaffold made of non-biodegradable polymers must be avoided to avoid chronic inflammation and nerve compression over time, and it is therefore preferable to use biodegradable materials. (7). Though in biodegradable materials, surface erosion must be considered over sudden erosion, because it allows the scaffolds to maintain structural integrity for a prolonged period after implant placement (8).

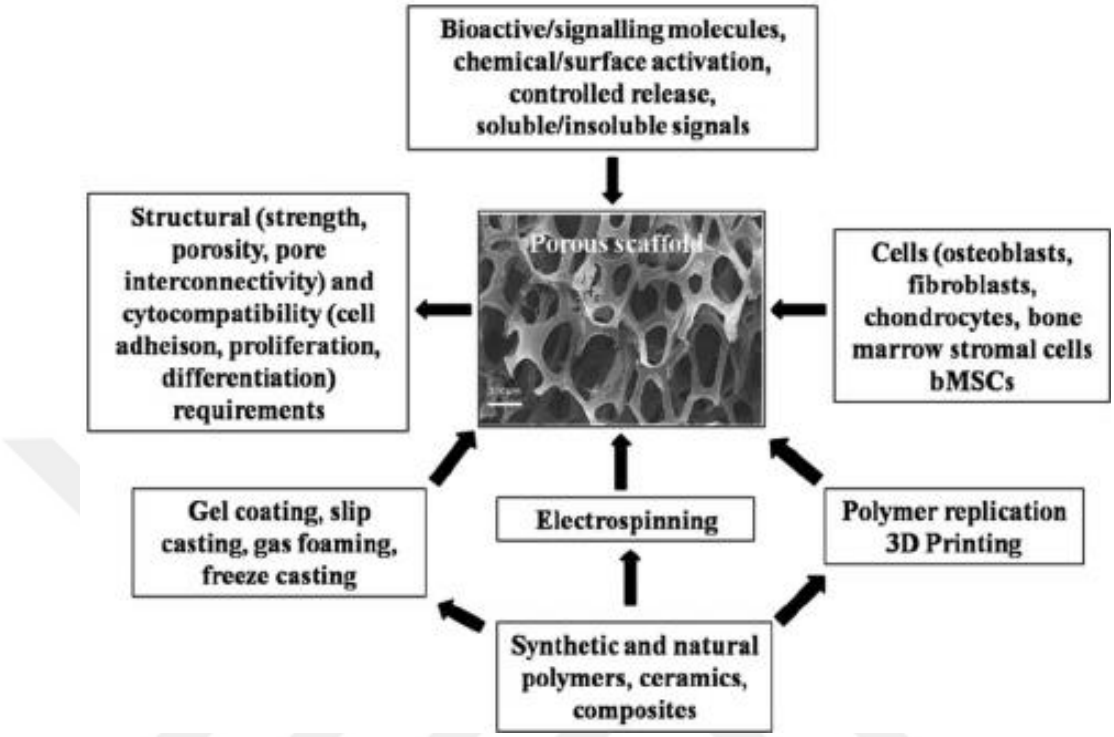

Figure 2.3. Different methodologies for creating porous scaffold structures (9).

Another strategy for bioactive scaffold design for nerve regeneration and tissue repair is using natural and synthetic polymer scaffolds together and creating a hybrid scaffold. By polymerization, cross-linking, and functionalization (modification by block structures, by blending, copolymerization) mixing the different kinds of polymer structure might result in successful experimental results Xiaoxiao et al. implies that to promote axonal guidance and attract migratory neuroblasts, electroactive graphenes could also be combined with other natural materials and built into bioactive scaffolds (10).

2.2.2. Hydrogel scaffolds

Hydrogels are three dimensional networks of polymeric materials which could absorb large amounts of water or fluids because of their hydrophilic nature. Their hydrophilic capacity comes from the presence of hydrophilic groups such as –OH, –CONH–, –$CONH_2$–, and –SO_3H in polymers forming those hydrogel structures. Due to the involvement of these chemical groups and domains in the polymeric network of hydrogel, the polymer is hydrated to different degrees (11).

Hydrogels are non-soluble networks if they go under a fixing process called crosslinking, which can be chemically (i.e., junctions, ionic interactions) or physically (i.e., entanglement). Hydrogels can be obtained from a respond to certain kinds of stimuli separately or combined, such as pH change, ionic interactions and temperature change (12).

Hydrogels are suitable forms of polymeric biomaterials for the use of tissue engineering because of their water uptake capacity, porous structure and proper biodegradability. Because of the high-water uptake capacity hydrogel scaffolds allows and helps with the nutrient exchange with the environment and the cells. The hydrogel structure with these characteristic features, it possesses elasticity and flexibility similar to natural extra cellular matrix (ECM) (2).

In literature, hydrogels outstand as mostly used biomimetic scaffold which has the ability to model natural living tissues. Its high-water levels and soft consistency are like the original tissue. Hydrogels can therefore be utilized as optical lenses, biosensor

membranes, linings to artificial hearts, scaffold fabrication elements, and drug delivery (13).

2.2.3. Polymers for hydrogel preparation

2.2.2.1. Hyaluronic acid based hydrogels

Hyaluronic acid is a non-sulphated glycosaminoglycan biopolymer found in the extracellular matrix of various soft connective tissues, consisting of alternating units of D- glucuronic acid and N-acetyl-D-glucosamine, linked together via alternating β-1,4 and β-1,3 glycosidic bonds (14). Hyaluronic Acid (HA) presence in the extracellular matrix (ECM) of the damaged or injured tissues implies its correlation with wound healing processes. In literature it has been reported that HA amount might expand rapidly at embryonic tissue damages without scarring as a result of decreased proinflammatory cytokines expression which oversee down regulation of hyaluronic acid synthesis in the organism. Hyaluronic acid is responsible for carrying needed materials and nutrients to the damaged area in the tissue owing to its excessive water uptake ability and help inflammatory signaling for tissue repair mechanisms (15). A wound environment abundant in HA may also enhance cell motility and proliferation, both of which are required for wound healing as reported by Chen et al. (16). The hyaluronic acid in the tissue keeps the tissue environment moist and the degraded HA in the scarred tissue promotes cell proliferation and migration. These features increases HA use in the biomedical applications with tissue engineering (17).

2.2.4. Cross-linking Strategies for Hydrogels

As mentioned above, there are several different cross-linking methods for hydrogels. In further detail they can be separated as stimuli-responsive hydrogels (smart hydrogels) and chemical responsive hydrogels. Stimuli responsive hydrogel can further classify as; temperature /thermo responsive hydrogels, photo/light responsive hydrogels, and electro- and magnetic responsive hydrogels. Moreover, chemical responsive hydrogels are pH responsive hydrogels, glucose responsive hydrogels and biochemical responsive hydrogels (18).

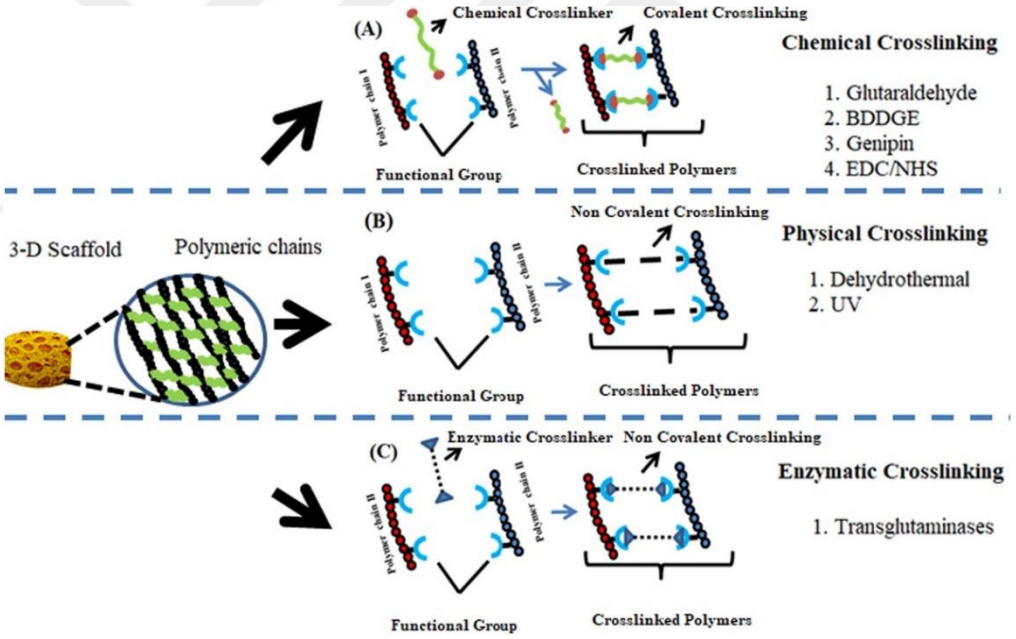

Figure 2.4. Cross-linking strategies for hydrogel scaffolds (18).

2.2.5. Photo-crosslinked hydrogels

Hydrogels that are responsive to light and crosslinkable via a light source are called photo-crosslinkable hydrogels. They have a big impact on biomedical applications. These types of hydrogels include a polymeric network and a photo initiator. Stimuli from the light source induces changes in the hydrogel's physical and chemical characteristics. The light signal is taken by the photo initiator molecules that transmits the photoirradiation to a chemical signal for crosslinking process. Most of the photo-crosslinkable hydrogel designs involve UV light and thus it may limit the application areas of these hydrogel scaffolds (19). UV light induced crosslinking is a simple, fast and non-toxic method for stabilizing the scaffolds. Also, it is beneficial for sterilizing the samples as the UV light disrupts the harmful microorganisms and makes the scaffold entirely sterile (20). Two different observable facts happen under UV exposure: crosslinking and UV-induced denaturation. The balanced exposure of these two facts determines the effects of UV to the prepared scaffolds (21).

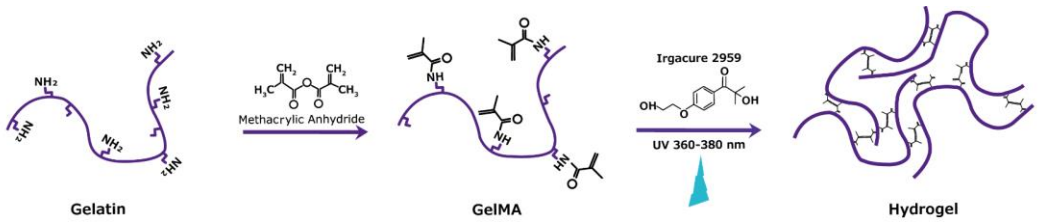

Figure 2.5. Synthesizing UV-crosslinked Gelatin-Methacrylate hydrogel (22).

It has been reported that methacrylated hyaluronic acid hydrogel irradiated via UV treatment increased the storage and elastic moduli of the gel with enhanced rigidity and intrinsic osteogenic effect by Poldervaat et al (23).

2.2.6. Bioactive hydrogels

2.2.6.1 Peptide-conjugated hydrogels

Biomaterials incorporating unique cell-adhesion compounds have the potential to affect tissue development and regeneration. Nevertheless, understanding the interactions of cells with biomaterials and related effects on tissue regeneration is crucial for appropriate tissue development. Extracellular matrix (ECM) component formation is one of them. Because of its impact on the sustainability of the outcome, the amount of ECM produced by cells proliferating on a scaffold is crucial for tissue development. The ability of nanomaterials to interact with biochemical and physiological systems determines their potential utility in biomedical applications (24).

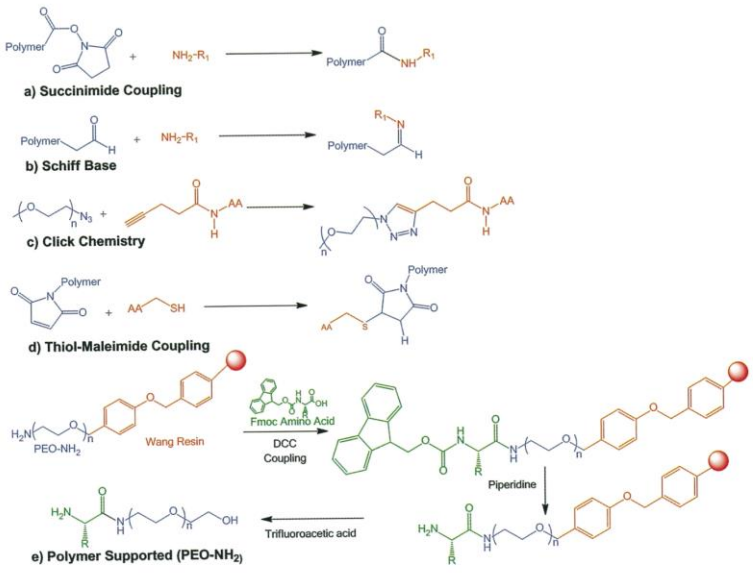

Figure 2.6. Chemical demonstration of some peptide polymer conjugation strategies (25)

Scaffolds can be designed to provide cells with adhesive capabilities for cell attachment (e.g., RGD, GFOGER, IKVAV). Sun et al. reports that *IKVAV* peptide (The sequence corresponds to Ile-Lys-Val-Ala-Val, respectively.) have been used in peptide-hydrogel conjugate usage for tissue regeneration. *IKVAV* is used to stimulate neuronal growth and axon regeneration purposes due to its laminin residues (26).

In another study in 2006, Gelain et al. reports that *RGD*-based sequences from fibronectin (*RGDS*), collagen VI (PRGDSGYRGDS), and laminin-derived motifs (*YIGSR, IKVAV, PDSGR*) may be used to develop a 3D cell culture system with mouse adult neural stem cells (27).

2.2.7. Hyaluronic acid Scaffolds for nerve tissue engineering

The interconnecting porosity nature of HA hydrogels allows nutrients to be transported to cells, nerve cells, and blood vessels (28). As a result, HA hydrogels are implanted to aid brain regeneration. In both the PNS and the CNS, HA has been shown to be helpful in minimizing scar formation and improving neuronal regeneration. (29,30)

Lin et al. suggests that treatment with HA hydrogels considerably reduced glial scarring, with significantly smaller gliosis thickness and fewer glial fibrillary acidic protein (GFAP)-positive cells around the scarring location (29). As shown in a new study, exclusively high-molecular-weight HA hydrogels exhibited the ability to prevent astrocytic activation, macrophage/microglia infiltration (31).

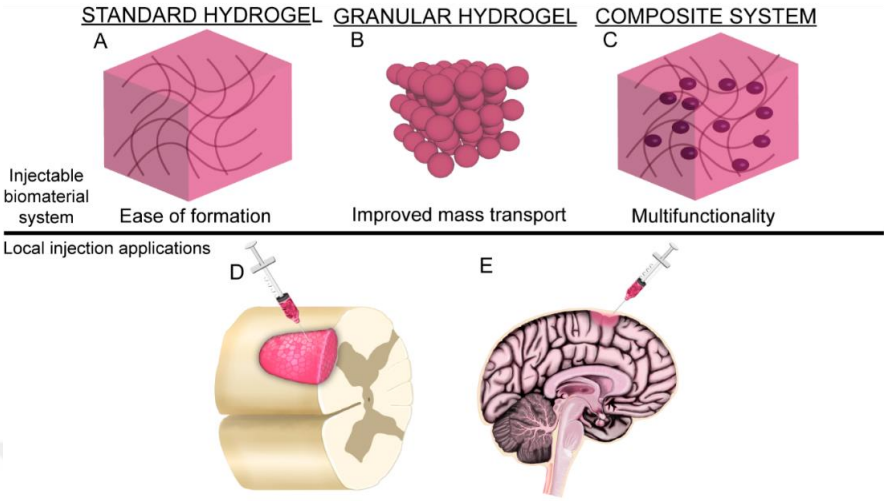

Figure 2.7. Different use and modification methods for Hyaluronic Acid usage in nerve tissue damage (32).

Spearmen et al. suggests that methacrylated HA can have a wide range of mechanical properties, allowing it to be used in a variety of soft tissues. Furthermore, the addition of different ECM components to these hydrogels can easily alter their properties. In addition to the modified HA, methacrylated HA can be used to create complex ECM-like scaffolds for a number of soft tissue engineering thanks to its adjustable foundation (33).

3. MATERIALS AND METHODS

3.1. Materials

Methacryloyl chloride (97%), Dimethyl Sulfoxide (DMSO) anhydrous (99%), Methacrylic anhydride (94%), Hyaluronic acid sodium salt, Maleimide-PEG6-succinimidyl ester, 2-Aminoethyl methacrylate hydrochloride (90%), Ibuprofen (98%), Dowex Mb Mixed Ion Exchange Resin, Tetrabutylammonium fluoride (TBA-F) 75 wt. % solution in water, Chloroform-d (99,8%), D, N, N-Dimethylformamide anhydrous (DMF) (99,8%) are purchased from Sigma-Aldrich. IKVAV-C peptide (95% purity) was purchased from Biomer. Pierce™ BCA Protein Assay Kit and Pierce™ Quantitative Fluorometric Peptide Assay Kit are purchased from Thermo Scientific. All other materials used are purchased from Sigma- Aldrich unless stated otherwise.

3.2. Methods

3.2.1. Synthesis and characterization of functional HA (HA-MA)

The hydrogel skeletal structure was composed of Hyaluronic Acid (HA), a natural and biocompatible polysaccharide. Methacrylate reactive groups were added to the side branches of hyaluronic acid polymer chains so that it can participate in the gelation step. For this purpose, the primary hydroxyl groups in the structure of the biopolymer were reacted with methacryloyl chloride (MAC) in an basic environment (34). After it was determined that the dissolution coefficient of hyaluronic acid sodium salt (HA) in dimethyl sulfoxide anhydride (DMSO) was low, another procedure was followed based

on literature (34). First, 100.0 mg of Hyaluronic Acid was dissolved in 100.0 mL of dH_2O to increase its solubility. 1 g of Dowex resin and 1mL of Tetra-n-butylammonium fluoride (TBA-F) were spun in 10mL of dH_2O on a magnetic stirrer at 300 rpm for 1 hour at room temperature. Then, the water and excess TBA-F solution were discarded and the remaining Dowex resin was washed 3 times with distilled water. The washed resin was transferred into 1% hyaluronic acid solution (w/v) and stirred at room temperature on a magnetic stirrer at 300 rpm for 2 hours. Then it was centrifuged at 5000 rpm for 3 minutes. The centrifuged samples were frozen at -80 °C in HA-TBA-F solution separated from the resin and lyophilized for 16 hours. 500.0 mg of the lyophilized HA-TBA-F was dissolved in 50 mL of anhydrous DMSO under nitrogenous environment.

To the mixture prepared in the second step, 100.0 mg of 4-Dimethylaminopyridine (DMAP) was dissolved in anhydrous DMSO and 155.0 µL of methacryloyl chloride (MAC) 1,34 mL of triethylamine were added again under nitrogenous environment into dissolved HA solution. The said mixture was stirred on a magnetic stirrer at 50 °C for 48 hours. Within the 2nd hour of mixing, 77.0 µL Hydrochloric Acid (HCl) was added as molar amount equal to the amount of DMAP and the pH of the media balanced as 8.0. After 48 hours, this solution was dialyzed against 150 mM sodium chloride at 4 °C for 3 days and then against deionized (DI) water for 4 days against a 3.5 kDa cut-off dialysis membrane, in order to remove excess molecules that did not react or any impurities in the environment. The material taken from the dialysis was frozen at -80°C, lyophilized and stored at 4°C.

Figure 3.1. Hyaluronic Acid-Methacrylate synthesis

In addition, a different protocol was followed for the addition of methacrylate reactive groups to the side branches of Hyaluronic Acid polymer chains (35,36).

In this protocol, 500 mg of HA was dissolved in 25 mL of dH_2O, placed under nitrogenous environment, and 4 mL of methacrylic anhydride was added. After making sure that the solutions were mixed, the pH of the mixture was fixed to 8 with 1 M sodium hydroxide (NaOH) and stirred at 5 °C for 24 hours on a magnetic stirrer. Then, the prepared solution was dialyzed against a 3.5 kDa membrane against double distilled water for 3 days for purification. The mixture taken from the dialysis membrane was transferred to a tube and frozen at -80 °C, lyophilized and stored at 4°C. The presence of characteristic functional groups of HA-MA was demonstrated by Fourier Transform-Near Infrared Spectroscopy (FT-IR) spectroscopy and amount of methacrylate groups in the HA-MA structure was determined by using proton Nuclear Magnetic Resonance (HNMR) and UV-Vis Spectrophotometer (37).

3.2.2. Preparation and characterization of HA based hydrogels

The prepared dry hyaluronic acid polymers HA-MA1(Methacryloyl Chloride) and HA-MA2 (Methacrylic anhydride) were dissolved in phosphate buffered solution (PBS) as 2% (w/v) and gelation experiments were carried out.

For gelation, 400.0 µL of 2% (w/v) HA-MA solutions and 0,1% and 0,05% (w/v) photo initiator (Irgacure I2959) in total solution were added and the mixture and was divided into 3 groups. First group was gelled under UV light (Analytik Jena US, 365nm,100 watt). Second group was gelled by adding 20.0 µL of 10% Ammonium persulfate (APS) and 2,4 µL of Tetramethyl ethylenediamine (TEMED) to the final

solution with and finally third (control) group left for gelation without UV light (365nm). All gel groups were checked at certain time points (5, 10, 15, 30 and 60 minutes).

As a result of gelation optimizations, the HA-MA1 protocol was modified. Protocol's material amounts changed as, 500.0 mg Hyaluronic Acid and 50.0 mL dH2O for dissolving HA, 9.0 mL TBA-F, 14.0mL dH2O for 2 g of Dowex resin for the first step as ion exchange of HA. After removing the Dowex resin this mixture was lyophilized. Lyophilized 1,75 g HA-TBA-F was dissolved in 175 mL anhydrous DMSO with 350.0 mg DMAP and 540.0 µL MAC and for the second step. Then this mixture was again lyophilized and stored at 4°C. The hyaluronic acid polymer obtained from the revised protocol was dissolved as 2% (w/v) HA-MA1 in PBS. For gelation, 300 µL HA-MA1 in two separate bottles and 0.5% of the total solution Irgacure I2959 and 2,2-dimethoxy-2-phenylacetophenone (DMPA) were added to the solution. Both mixtures were controlled under UV light for certain periods (5,10,15,30,60 minutes). Gelation was not observed as a result of gelation experiments.

To control the used photoinitiator activities, 100% undiluted Poly (ethylene glycol) dimethacrylate (PEGdiMA) solution was tried. In a vial 300 µL PEGdiMA and as 0,5% in total solution Irgacure I2959 was added. In another vial same amounts of PEGdiMA and Dimethylol propionic acid (DMPA) was added. These vials were left for gelation under UV (365nm) light.

To control UV (365nm) efficiency to 300 µL PEGdiMA solution 20 µL of 10% Ammonium persulfate (APS) and 2,4 µL Tetramethyl ethylenediamine (TEMED) was added. Although, this vial never received any UV light. It was controlled for certain periods (5,10,15,30,60 minutes) without UV light. Gelation was observed in the vials prepared with DMPA and APS&TEMED.

Then, HA-MA2 obtained from the second procedure was tested for gelation with HA-MA1. While testing this material, it was decided to increase the photo initiator concentration to 3% in gel trials, since the amount of crosslinker in the first trials was deemed insufficient.

The hyaluronic acid polymer HA-MA1 and HA-MA2 from the first and second protocol were dissolved in PBS as 2% (w/v). For gelation, 400µl HA-MA1 was put in two separate vials. To first vial 3% in total solution photo initiator Irgacure I2959 was added. To second vial 3% in total solution DMPA was added and both mixtures were controlled under UV light for certain periods (5,10,15,30,60 minutes).

Then 400µl HA-MA2 was put in two separate vials. To first vial 3% in total solution photo initiator Irgacure I2959 was added. To second vial 3% in total solution DMPA was added and both mixtures were controlled under UV light for certain periods (5,10,15,30,60 minutes).

Gelation was observed in both HA-MA solutions, but it was decided that the HA-MA2 polymer obtained with the second protocol was more useful in terms of time and material savings. It was decided to use HA-MA2 in the next gelation trials. However, it was decided to continue using DMPA instead of Irgacure I2959 as a crosslinker, since the use of DMPA in gel trials is more effective in terms of obtaining more stable results. Results can be seen in Table 4.1.

Prepared hydrogel structures were analyzed in terms of physical, chemical, morphological and mechanical properties using the following characterization methods (11).

Determination of water uptake capacity and gel conversions: The hydrogels were dried by the lyophilization method and incubated in water. At certain time intervals, hydrogels were removed from the beaker and excess water was liberated quickly. The they were weighed as swollen gel (Ws) and compared with the weight of the initial dry state (Wd). Thus, the time dependent water holding capacity of hydrogels is calculated as the formula given:

$$\%\ Swelling\ Ratio = \frac{Ws - Wd}{Wd}\ x\ 100 \qquad \text{(Eq.1)}$$

Gel conversions of the prepared hydrogels are calculated as the formula given:

$$\%Gel\ conversion = \frac{Weight\ of\ obtained\ dry\ gel\ (Wd)}{Dry\ weight\ of\ all\ materials}\ x\ 100 \qquad \text{(Eq.2)}$$

Determination of mechanical properties: The hardness and flexibility properties of the prepared hydrogels were measured with Malvern Kinexus rheometer instrument with UV curing property. During these measurements, degradation time and point were measured.

Degradation properties of hydrogel were measured with J2 SR 4703 SS geometry. Degradation property was studied by taking measurements at parameters between γ = 0.001 and γ =1 at f = 1 Hz at 37 ºC. The gelation process was analyzed under CD-auto

strain mode with $\gamma = 0.01$ at $f = 1$ Hz The strain-dependent oscillatory rheology and frequency dependent oscillatory rheology of hydrogel scaffolds were tested at 1 Hz and $\gamma = 0.01$ at 37 °C to mimic the body conditions (38).

Morphological analysis: These hydrogel scaffolds, which are expected to have a porous structure, were visualized using Scanning Electron Microscopy (SEM) for their porosity and pore sizes. The semi-quantitative elemental analysis was done with scanning electron microscopy (SEM) (Thermo Quattro S) coupled with energy dispersive x-ray spectroscopy (EDS) (EDAX) detector. Lyophilized hydrogels were coated with 20 nm of gold (Au/Pb) under vacuum. After Au coating, the semi-quantitative elemental analysis of the hydrogel samples was examined under high vacuum.

Functional group analyses: The characteristic functional groups of the chemical structures of prepared hydrogels were determined by the Thermo^{TM} Nicolet iS10 FT-IR (Thermo Fisher).

Spectrophotometric analyses: Spectrophotometric analyses were conducted with Shimadzu UV-VIS 2600.

3.2.3. Synthesis and characterization of peptide monomer (IKVAV-MA)

The peptide sequence, IKVAV, desired to be conjugated into the hydrogel structures was purchased as containing cystine amino acid at one end with a free thiol group so that they can participate in the gelation process.

The peptide-containing monomer was obtained by using an intermediate linker molecule (Maleimide-PEG6-succinimidyl ester) with two different functional groups. In this intermediate linker molecule, there is one methacrylate reactive group that participated in photo-polymerization, and one maleimide reactive group that can be covalently bonded with the peptide sequence. Therefore, one peptide sequence can be included in each reactive monomer.

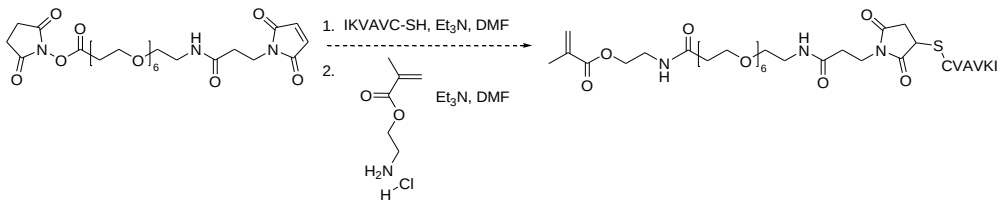

Figure 3.2. IKVAV-MA synthesis

First, stock solutions of reagents to be used in the synthesis of peptide-containing monomer were prepared in anhydrous dimethyl formamide (DMF) as a solvent: 1,84 µL triethylamine (Et_3N) in 500 µL DMF and 1,321 mg 2-Aminoethyl methacrylate hydrochloride (NH_2-HCl) in 500 µL DMF under nitrogenous environment in two different bottles.

The reaction was carried out in two stages. Firstly, Maleimide-PEG6-succinimidyl ester was weighed 3,97 mg and dissolved in 400 µL DMF anhydride in nitrogenous environment.

In the second step, 5 mg of IKVAV-C peptide was weighed and dissolved in 500 µL DMF anhydride in nitrogenous environment. These two solutions were taken into a 10 mL round-bottom flask without disturbing the nitrogenous environment. In the last step, 50 µL from prepared Et_3N stock, which was also in nitrogenous environment, was added. The reaction was stirred at 300 rpm in a magnetic stirrer for 2 hours at room temperature. In the second stage of the reaction, 50 µL of triethyl amine (Et_3N) and 2-Aminoethyl methacrylate hydrochloride (NH_2-HCl) stocks in nitrogen environment were taken and added to the main reaction flask. The reaction was stirred at 300 rpm in a magnetic stirrer for 24 hours at room temperature. The prepared solution was dropped on diethyl ether at -20 °C the next day, then centrifuged at 5000 rpm for 2 minutes and precipitated. After precipitation, diethyl ether was separated, and the material was left to dry under a high vacuum valve for 2 hours. The dried material was stored at -20 °C.

This peptide monomer was purified using HPLC column chromatography with C18 column (Agilent VariTide RPC 250x10 mm ID). The column equilibrated by 5% mobile phase (B solution was Acetonitrile A solution was dH_2O containing 0,025% Trifluoracetic acid) and its chemical structure was characterized using HNMR and FT-IR spectroscopies (39).

3.2.4. Preparation and characterization of drug-loaded hydrogels with the prepared reactive Hyaluronic acid polymer

Lyophilized HA-MA2 was dissolved as 3% (w/v) in DI water. Then 500 µL of this dissolved HA-MA2 was frozen -80 °C, then lyophilized in 4 different vials. Then, 40 mg of DMPA was dissolved in 200 µL acetone as photoinitiator stock solution. After, 40 mg of Ibuprofen was dissolved in 1000 µL acetone as the drug stock solution. Then, Ibuprofen drug from stock (40 mg/mL) was added on dry HA-MA2 for H1, H2, H3, respectively as, 2.5 mg, 5 mg, 10 mg in total solution. Afterwards, 25 µL photoinitiator DMPA as 1% in the total solution was added to the vials. To complete the total volume of vial to 500 µL dH_2O was added.

The chemicals in the solution are left for gelation by the photopolymerization method based on the free radical polymerization mechanism under UV light for 1 hour (365 nm) (37). After crosslinking the hydrogels are washed using DI H_2O respectively and purified by removing unreacted chemicals. After washing steps, hydrogels are dried and lyophilized again for storage at 4 °C.

Table 3.1. Composition of the control and drug loaded hydrogels

H0	H1	H2	H3
500 µL HA-MA dry	500 µL HA-MA dry	500 µL HA-MA dry	500 µL HA-MA dry
25 µL photoinitiator	25 µL photoinitiator For 2.5 mg	25 µL photoinitiator For 5 mg	25 µL photoinitiator For 10 mg
No Drug	Ibuprofen 62.5 µL	Ibuprofen 125 µL	Ibuprofen 250 µL
475 µL dH_2O	402.5 µL dH_2O	350 µL dH_2O	225 µL dH_2O

Prepared hydrogel structures were analyzed in terms of physical, chemical, morphological and mechanical properties using the following characterization methods (11).

Determination of water uptake capacity and gel conversions: The hydrogels were dried by the lyophilization method and incubated in water. At certain time intervals, hydrogels were removed from the beaker and excess water was liberated quickly. The they were weighed as swollen gel (Ws) and compared with the weight of the initial dry state (Wd). Thus, the time dependent water holding capacity of hydrogels is calculated as the formula given:

$$\%\ \text{Swelling Ratio} = \frac{\text{Ws} - \text{Wd}}{\text{Wd}}\ \text{x}\ 100$$

(Eq.1)

Gel conversions of the prepared hydrogels are calculated as the formula given:

$$\%\text{Gel conversion} = \frac{\text{Weight of obtained dry gel (Wd)}}{\text{Dry weight of all materials}}\ \text{x}\ 100$$

(Eq.2)

Determination of mechanical properties: The hardness and flexibility properties of the prepared hydrogels were measured with Malvern Kinexus rheometer instrument with UV curing property. During these measurements, degradation time and point were measured.

Degradation properties of hydrogel were measured with J2 SR 4703 SS geometry. Degradation property was studied by taking measurements at parameters between γ = 0.001 and γ =1 at f = 1 Hz at 37 ºC. The gelation process was analyzed under CD-auto strain mode with γ = 0.01 at f = 1 Hz The strain-dependent oscillatory rheology and frequency dependent oscillatory rheology of hydrogel scaffolds were tested at 1 Hz and γ = 0.01 at 37 °C to mimic the body conditions (38).

Morphological analysis: These hydrogel scaffolds, which are expected to have a porous structure, were visualized using Scanning Electron Microscopy (SEM) for their porosity and pore sizes. The semi-quantitative elemental analysis was done with scanning electron microscopy (SEM) (Thermo Quattro S) coupled with energy dispersive x-ray spectroscopy (EDS) (EDAX) detector. Lyophilized hydrogels were coated with 20 nm of gold (Au/Pb) under vacuum. After Au coating, the semi-quantitative elemental analysis of the hydrogel samples was examined under high vacuum.

Functional group analyses: The characteristic functional groups of the chemical structures of prepared hydrogels were determined by the Thermo^{TM} Nicolet iS10 FT-IR (Thermo Fisher).

Spectrophotometric analyses: Spectrophotometric analyses were conducted with Shimadzu UV-VIS 2600.

3.2.5. Determination of drug release profiles from hydrogel structures

In order to determine the release kinetics of the drug molecules entrapped in the hydrogel structures, three different amounts of drug were determined first. These are divided into 4 groups as H0 (control group), H1, H2, H3. As mentioned in section 3.2.4. (Table 3.1).

The release profiles of the dried hydrogels were determined by incubating at 37 °C and 10 mM PBS buffer solution pH 7.4 and acetic acid buffer solution pH 5.5. For each group, 5 mg of dry hydrogel is placed into the dialysis membrane (Mwt cut-off: 1 kDa) and incubated at 37 °C and. 150 rpm on an orbital shaker. Again, in order to provide body conditions, buffer solutions that are at least 10 times the volume of the dialysis bag were used as receptor solutions in these experimental set-ups, and "sink condition" was provided for drug release experiments. As buffer solutions, 40 mL acetic acid and 40 mL PBS were used. At certain time intervals (15 min,30 min, 45 min, 60 min,120 min...) samples were collected. The amounts of drug molecules released from the hydrogels and transferred to the outer receptor solution were determined using LC-MS (liquid chromatography-mass spectrometry). Spectrometric analyses were conducted by LC/LC-MS Agilent Technologies.

For LC-MS/MS analysis, free drug molecules were analyzed in the first step. Ibuprofen solution was prepared at a concentration of 2500 ppb and given to the device at a flow of 0.5 mL/min for 1 minute with stationary phase C18 prep-HPLC column and mobile phase 50% ACN: 50% H20 (40).

After introducing ibuprofen to the LC-MS/MS device and creating a method suitable for this molecule, a calibration curve was drawn using this method in order to quantify the molecule (41). For this, ibuprofen solutions at different concentrations were prepared by serial dilution method. These samples were analyzed using the method prepared from low to high concentration.

Encapsulation efficiency (EE %) was calculated using below formula: where Wt is the total amount of drug in the obtained release media and Wi is the total quantity of drug added initially during preparation. (Table 4.4)

$$\text{Encapsulation efficiency (EE\%)} = \frac{\text{Wt}}{\text{Wi}} \text{ x } 100 \quad \text{(Eq.3)}$$

This method and this calibration curve prepared according to determine the amount of free drug in the samples collected at different time points in drug release experiments (40). After the drug release experiments, all collected samples were analyzed in the LC-MS/MS device using the same method. The calibration curve of the free drug Ibuprofen was drawn using the software in this device, and then the files of the samples were evaluated on this curve. The concentration values obtained were calculated as a percentage for each hydrogel based on the amount of drug, they initially encapsulated.

3.2.6. Preparation of bioactive hydrogels with IKVAV-MA peptide monomer conjugated

Lyophilized 15 mg of HA-MA2 was dissolved as 3% (w/v) in 500 µL DI water. Then dissolved HA-MA2 vial was frozen -80 °C, then lyophilized again. Then, 40 mg of DMPA was dissolved in 200 µL acetone as photoinitiator stock solution. After, 1,5

mg of IKVAV-MA monomer was dissolved in 25 µL acetone. Afterwards, 25 µL photoinitiator DMPA as 1% in the total solution was added to the vials. To complete the total volume of vial to 500 µL dH_2O was added.

The chemicals in the solution are left for gelation by the photopolymerization method based on the free radical polymerization mechanism under UV light for 1 hour (365 nm) (37). After crosslinking the hydrogels are washed using DI H_2O respectively and purified by removing unreacted chemicals. After washing steps, hydrogels are dried and lyophilized again for storage at 4 °C.

3.2.7. Characterization of the obtained bioactive hydrogels

Determination of water uptake capacity and gel conversions: The hydrogels were dried by the lyophilization method and incubated in water. At certain time intervals, hydrogels were removed from the beaker and excess water was liberated quickly. The they were weighed as swollen gel (Ws) and compared with the weight of the initial dry state (Wd). Thus, the time dependent water holding capacity of hydrogels is calculated as the formula given:

$$\%\, Swelling\ Ratio = \frac{Ws - Wd}{Wd}\ x\ 100$$

(Eq.1)

Gel conversions of the prepared hydrogels are calculated as the formula given:

$$\%Gel\ conversion = \frac{Weight\ of\ obtained\ dry\ gel\ (Wd)}{Dry\ weight\ of\ all\ materials}\ x\ 100$$

(Eq.2)

Determination of mechanical properties: The hardness and flexibility properties of the prepared hydrogels were measured with Malvern Kinexus rheometer instrument with UV curing property. During these measurements, degradation time and point were measured.

Degradation properties of hydrogel were measured with J2 SR 4703 SS geometry. Degradation property was studied by taking measurements at parameters between γ = 0.001 and γ =1 at f = 1 Hz at 37 ºC. The gelation process was analyzed under CD-auto strain mode with γ = 0.01 at f = 1 Hz The strain-dependent oscillatory rheology and frequency dependent oscillatory rheology of hydrogel scaffolds were tested at 1 Hz and γ = 0.01 at 37 °C to mimic the body conditions (38).

Morphological analysis: These hydrogel scaffolds, which are expected to have a porous structure, were visualized using Scanning Electron Microscopy (SEM) for their porosity and pore sizes. The semi-quantitative elemental analysis was done with scanning electron microscopy (SEM) (Thermo Quattro S) coupled with energy dispersive x-ray spectroscopy (EDS) (EDAX) detector. Lyophilized hydrogels were coated with 20 nm of gold (Au/Pb) under vacuum. After Au coating, the semi-quantitative elemental analysis of the hydrogel samples was examined under high vacuum. To verify the peptide existence, the elemental ratios of carbon (C), oxygen (O), nitrogen(N) and sulfur (S) atoms were recorded.

Functional group analyses: The characteristic functional groups of the chemical structures of prepared hydrogels were determined by the Thermo^{TM} Nicolet iS10 FT-IR (Thermo Fisher).

Spectrophotometric analyses: Spectrophotometric analyses were conducted with Shimadzu UV-VIS 2600.

3.2.8. Determination of peptide amount in hydrogels

To determine the peptide amounts in bioactive hydrogel structures, two different methods and kits were used to get a correlated result with the assumed calculation.

Firstly, to determine peptide amount Pierce BCA Protein Assay Kit was used. All standards were prepared according to the commercially obtained kit manual. 1 ml of the working solution was added on top of dry hydrogel and mixed immediately. Sample was incubated for 30 minutes in water bath temperature set to 37 ℃ and then returned to room temperature. Measurement of absorbance was done at 562 nm using a UV-Vis spectrophotometer. The peptide amount was calculated using the calibration curve in the software of equipment.

Then, to determine peptide amounts embedded in the prepared dry bioactive hydrogels with Pierce^{TM} Quantitative Fluorometric Peptide Assay by Thermo Scientific^{TM}. The final concentration of the standard A was 841 μM for individual peptide concentration measurement and used as stock standard solution. All standards were prepared according to the commercially obtained kit manual. 10 μL of each assay

standard and hydrogel samples were pipetted into 96-well black plate. 70 µL of Fluorometric Peptide Assay Buffer was added on top of the assay standards and hydrogel samples. 20 µL of Fluorometric Peptide Assay Reagent were added into each well. Samples and the standards were incubated at room temperature for 5 minutes in dark. Fluorometric measurement were done at Ex/Em 390 nm/475 nm. To convert the concentration of the IKVAV-C samples from µM to µg/mL the following equation was used:

$$\text{Concentration } (\mu g/mL) = \text{ Mwt of Peptide (Da) x Concentration } (\mu M)/10^6 \quad \text{(Eq.3)}$$

3.2.9. Printing of bioactive hydrogels using 3D printing technology

Prepared hydrogel mixture was printed using AxolotlBio 3D Bioprinter with two heads. Separate heads' syringes were filled with non-dyed 3% HA-MA and methylene blue dyed 3% HA-MA with 1% photoinitiator DMPA. Prepared hydrogels were printed with printing speed of 6mm/s and feed ratio of 25%. Then printed shapes held under UV light (365nm) for 20 minutes. To control the crosslinking the printed shape was dipped into water and visually observed. (Figure 4.28).

4. RESULTS

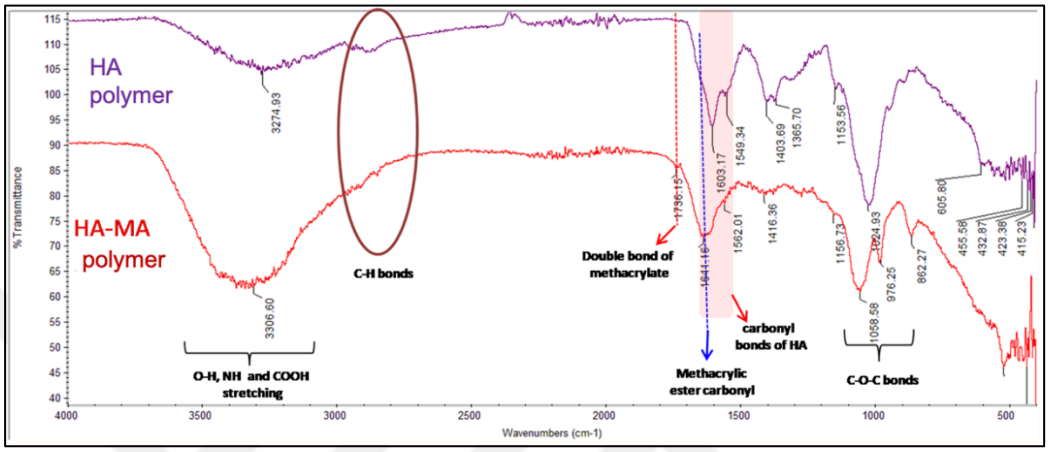

Figure 4.1. HA and HA-MA polymer FT-IR results

In order to show the presence of methylate groups in the chemical structure of HA-MA polymer, the peaks obtained in FT-IR spectroscopy were compared with the pure HA polymer peaks.

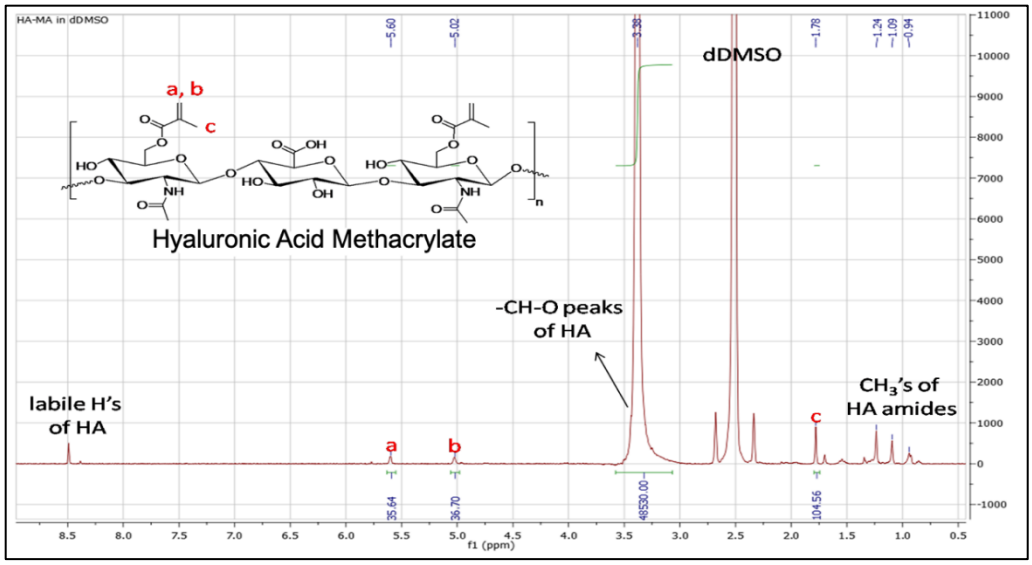

Figure 4.2. H-NMR spectroscopy result. of HA-MA

The proton NMR Spectroscopy method was used for the presence of methacrylate groups attached to the side branches of the HA polymer and the rate of bonding to the HA polymer by weight (42). The proton NMR spectrum of HA-MA polymer dissolved in dDMSO and analyzed in 128 scans is shown in Figure 4.2.

Table 4.1. Compositions of prepared HA-MA hydrogels and their results

Sample No	Composition	UV (365 nm) & Result
1	300 µL 100% PEGdiMA 20 µL 10% APS 2.4 µL TEMED	Not implemented Gelation observed
2	300 µL 2% HA-MA Dowex 20 µL 10% APS 2.4 µL TEMED	Not implemented Gelation not observed
3	300 µL 100% PEGdiMA 0.5% DMPA	Implemented Gelation observed
4	300 µL 100% PEGdiMA 0.5% Irgacure	Implemented Gelation not observed
5	300 µL 2% HA-MA Dowex 0.5% DMPA	Implemented Gelation not observed
6	300 µL HA-MA Dowex 0.5% Irgacure	Implemented Gelation not observed
7	300 µL 2% HA-MA Dowex 3% DMPA	Implemented Gelation observed
8	300 µL 2% HA-MA anhydride 3% DMPA	Implemented Gelation observed
9	300 µL 2% HA-MA anhydride 3% Irgacure	Implemented Gelation observed

Results of the HA-MA hydrogel optimization for formulation can be seen in Table. 4.1

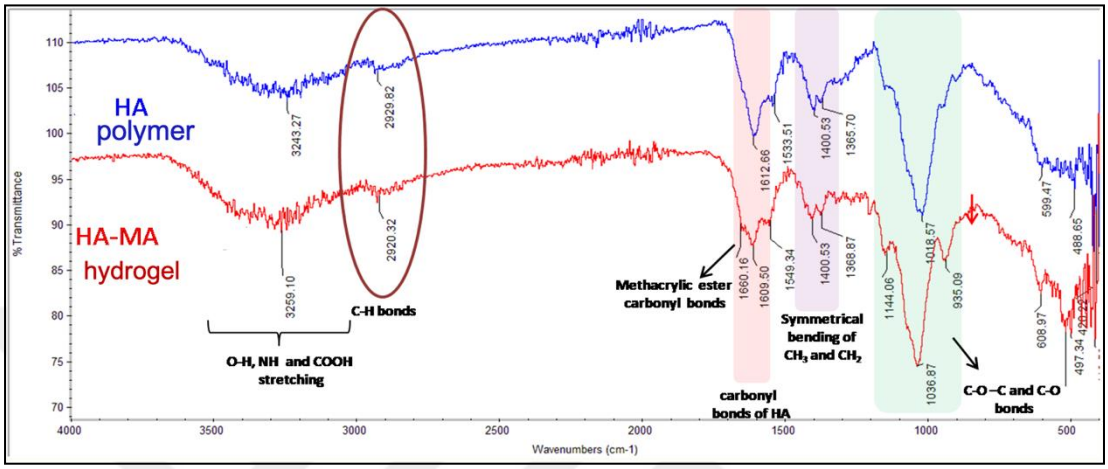

Figure 4.3. FT-IR spectrum of the prepared HA-MA hydrogel and comparison with pure HA

Chemical characterization of the prepared HA-MA hydrogel was performed using FT-IR Spectroscopy. The hydrogel, which was also lyophilized and stored in a dry form, was analyzed with the FT-IR device by taking the air as a background. Figure 4.3

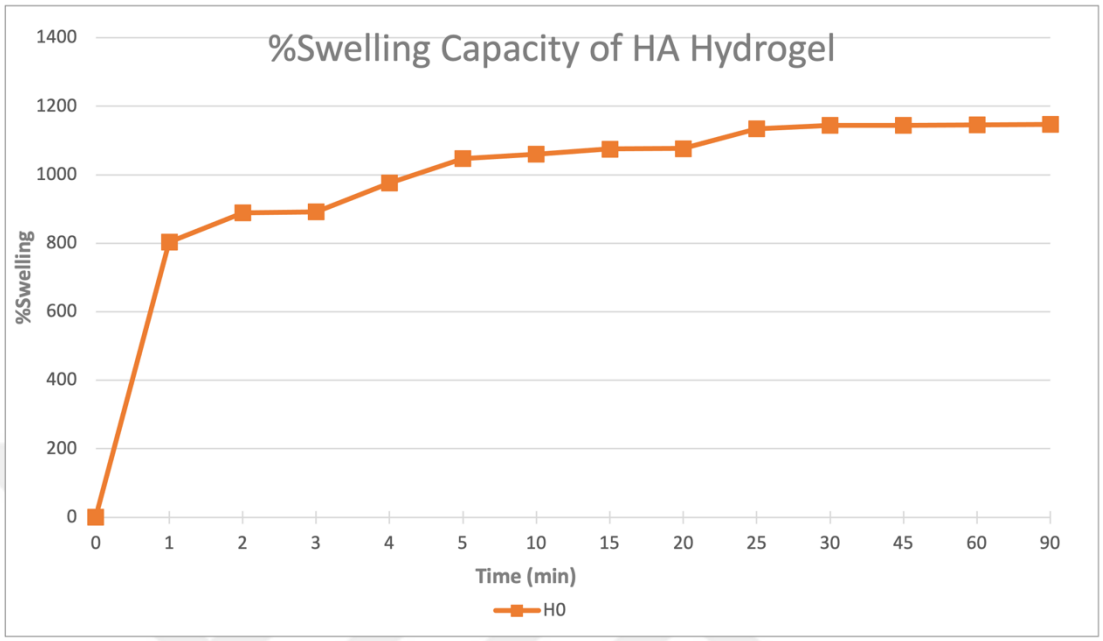

Figure 4.4. Swelling Capacity Curve for HA-MA (H0) hydrogel

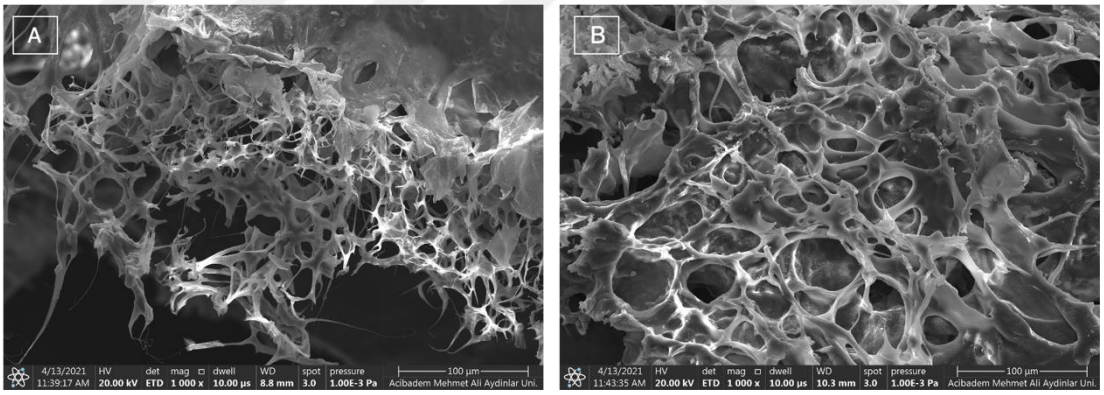

Figure 4.5. SEM images of HA-MA (H0) hydrogel A) Cross-section with a 45-degree angle B) Cross-section image of 90-degree angle

The morphological structure of the prepared HA-MA hydrogel was made using Scanning Electron Microscopy (SEM- Thermo QuatroS).

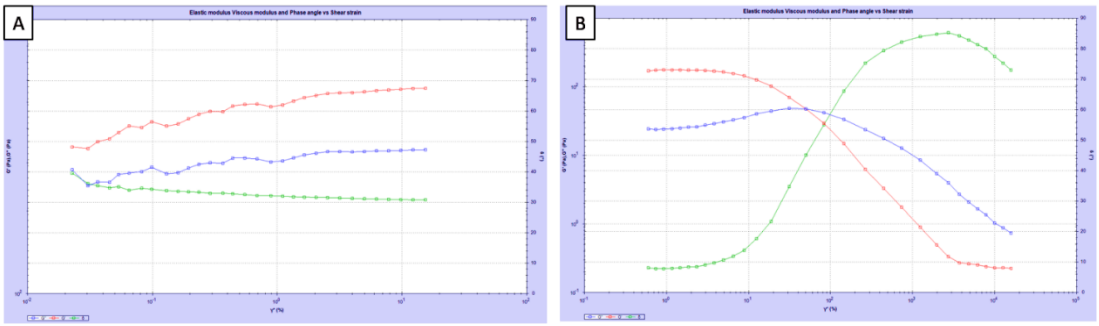

Figure 4.6. Rheometer analysis results of prepared HA-MA and control HA hydrogels (3%)

The mechanical strength of the obtained drug-loaded hydrogels was investigated using a rheometer device. The method and device parameters specified in methods (43).

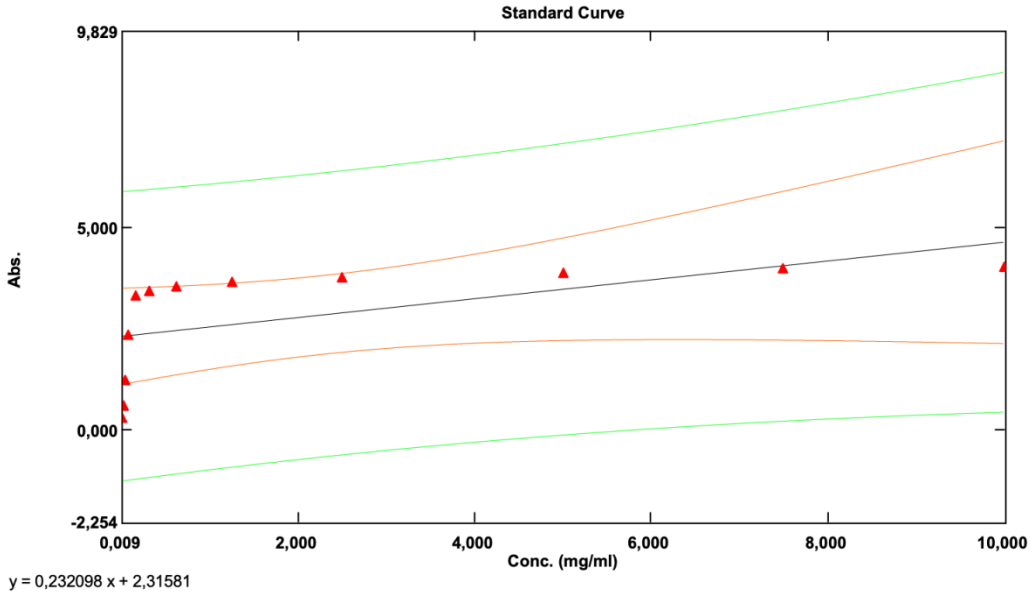

Figure 4.7. UV-Vis Calibration Curve for PEG-MA taken at 208 nm with PBS as a solvent

Table 4.2. Results for methacrylate group quantification obtained via UV-VIS Spectrophotometer at 208 nm from PEGMA standard curve

Sample ID	Conc	WL208
2% HA-MA2	9.577	4.539
2% HA-MA1	11.830	5.061
0.25% HA-MA2	6.323	3.783
0.25% HA-MA1	6.838	3.903

HA-MA 2% as HA-MA2 meaning 2% HA-MA methacrylic anhydride, HA-MA1 2% as HA-MA1 meaning HA-MA with methacryloyl chloride.

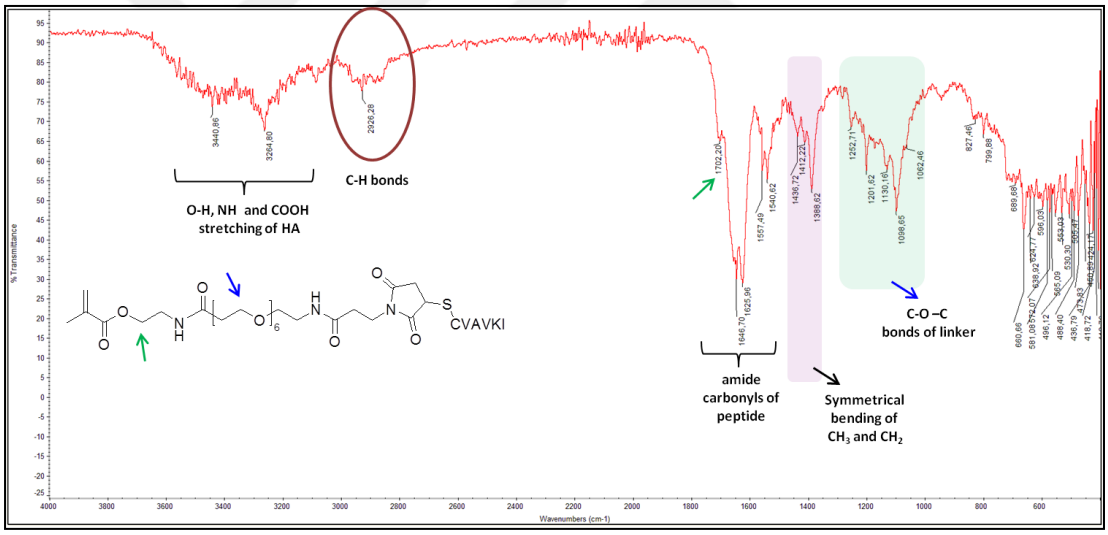

Figure 4.8. IKVAV-MA monomer FT-IR spectra result.

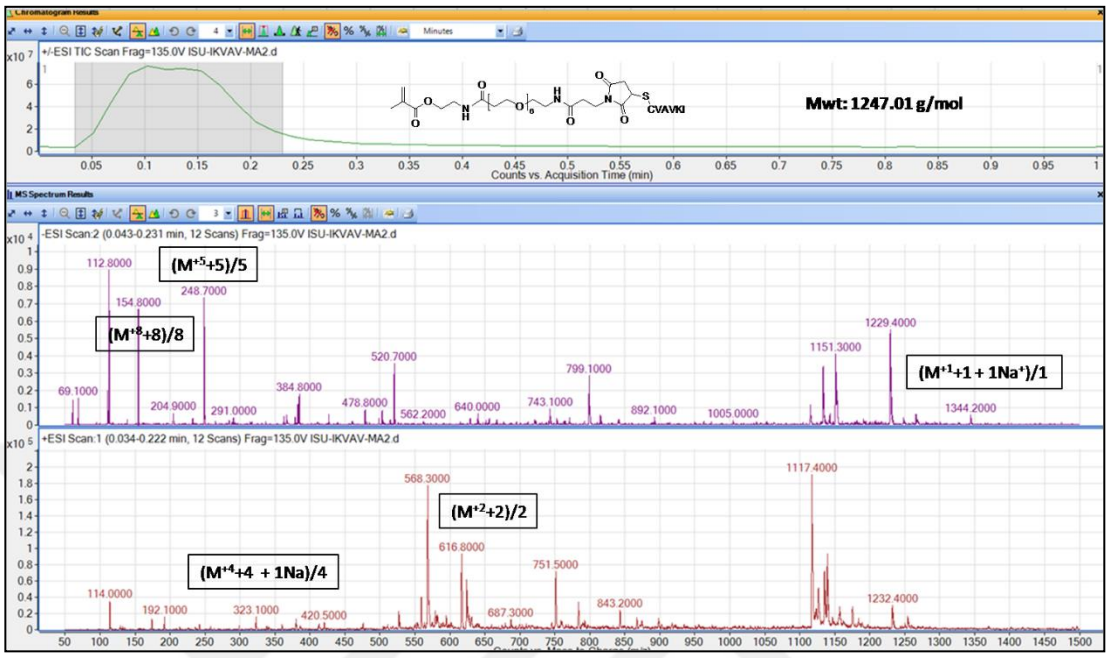

Figure 4.9. LC-MS/MS analysis result of IKVAV-methacrylate (IKVAV-MA) monomer

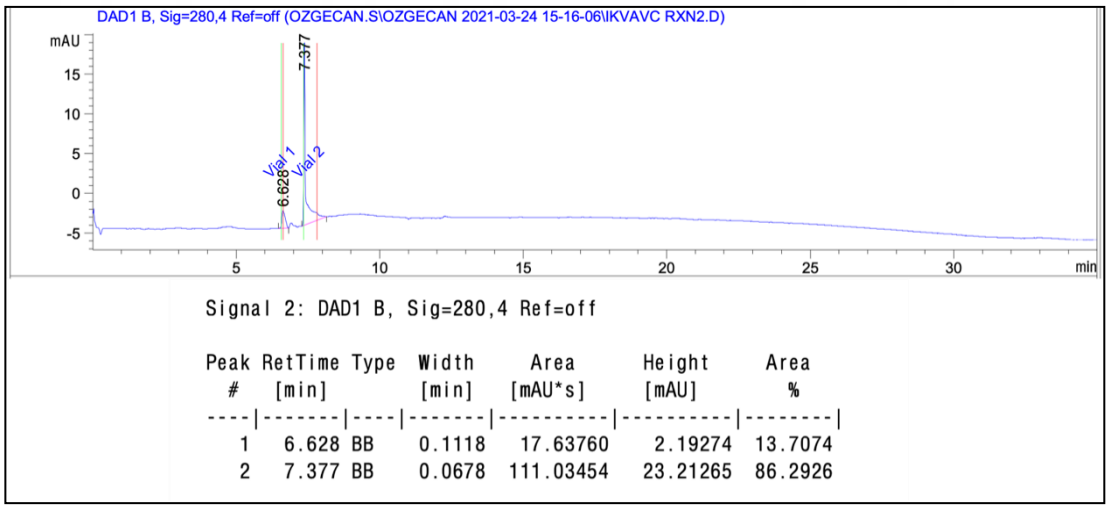

Figure 4.10. HPLC analysis result of IKVAV-methacrylate (IKVAV-MA) monomer

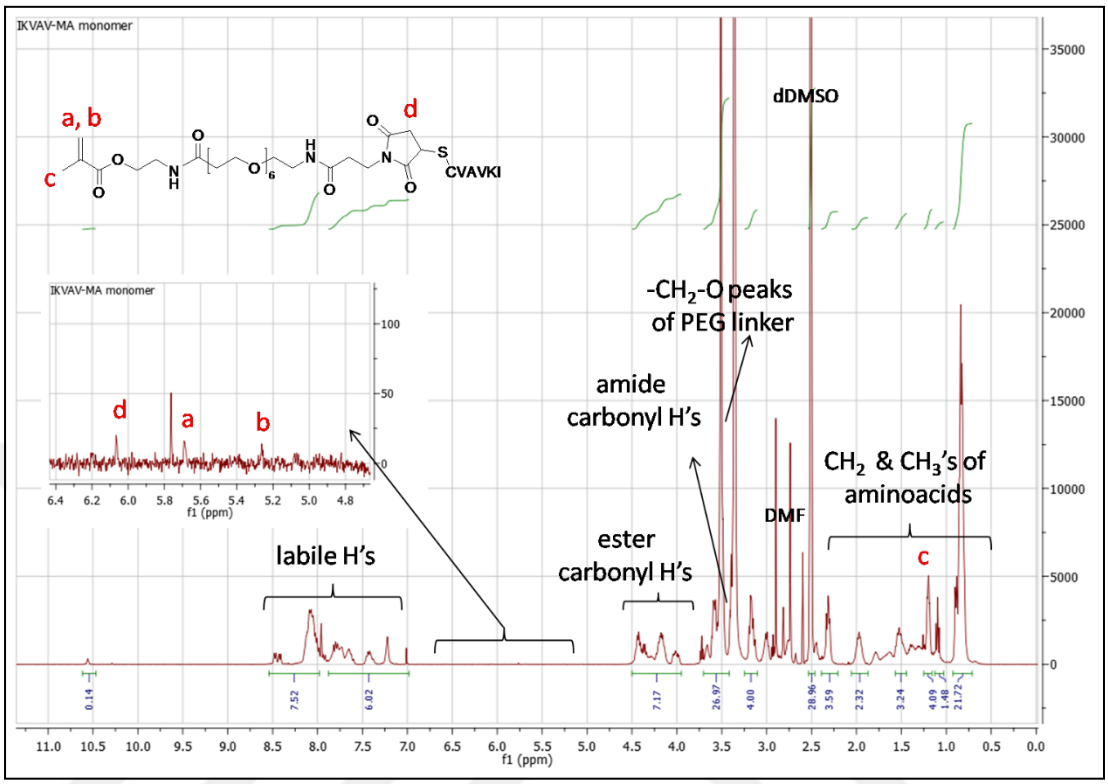

Figure 4.11. HNMR analysis result of IKVAV-methacrylate (IKVAV-MA) monomer

Table 4.3. Gel conversion rate of prepared HA-MA and drug loaded HA-MA hydrogels

Gel Groups	% Gel Conversion
H0	78.02607076
H1	55.94059406
H2	30.87378641
H3	37.11551606

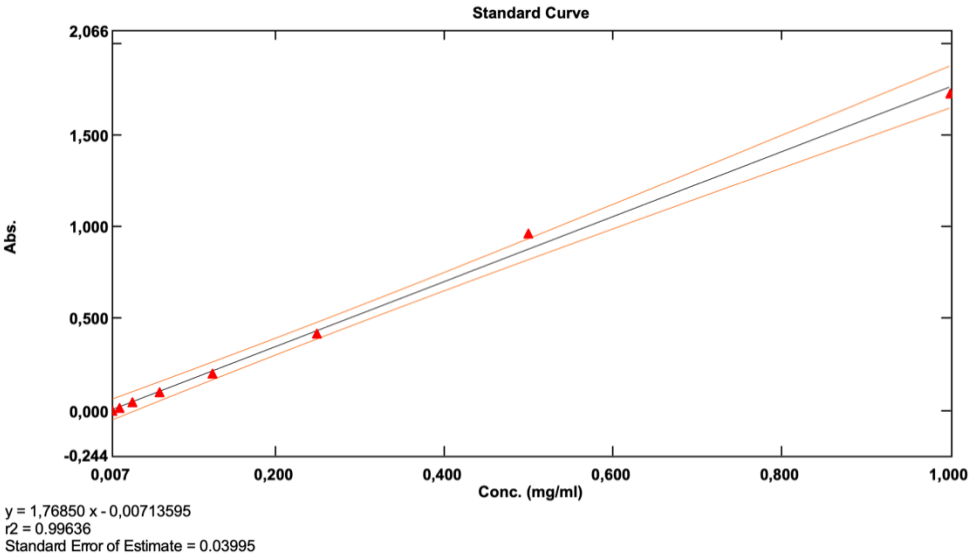

Figure 4.12. Calibration curve for Ibuprofen taken via UV-VIS Spectrophotometer at 264 nm

UV-Vis spectrophotometer device was used to calculate the amount of drug loaded on these hydrogels. First, the free drug Ibuprofen was prepared at different concentrations in 50% ACN and absorbance values were measured at the maximum wavelength of 264 nm (44). Then, a calibration curve was drawn that relates these absorbance values to the concentration (Figure 4.12). The amount of drug in these washing solutions was determined by using the calibration curve drawn for the free drug. This value was compared with the amount of drug used initially while preparing the hydrogels and the encapsulation efficiency was calculated separately for each hydrogel (Table 4.5.).

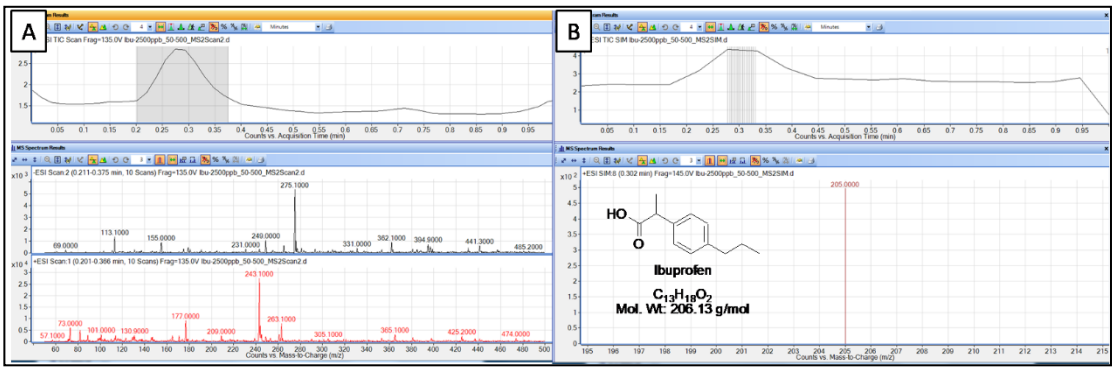

Figure 4.13. LC-MS/MS analysis results for free drug molecule

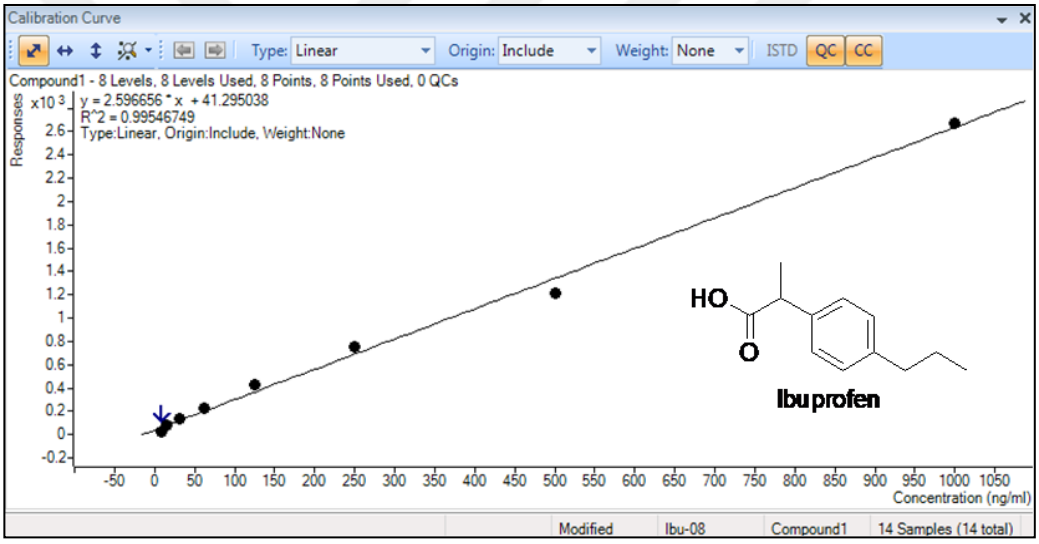

Figure 4.14. Calibration curve plotted by LC-MS/MS for free drug molecule

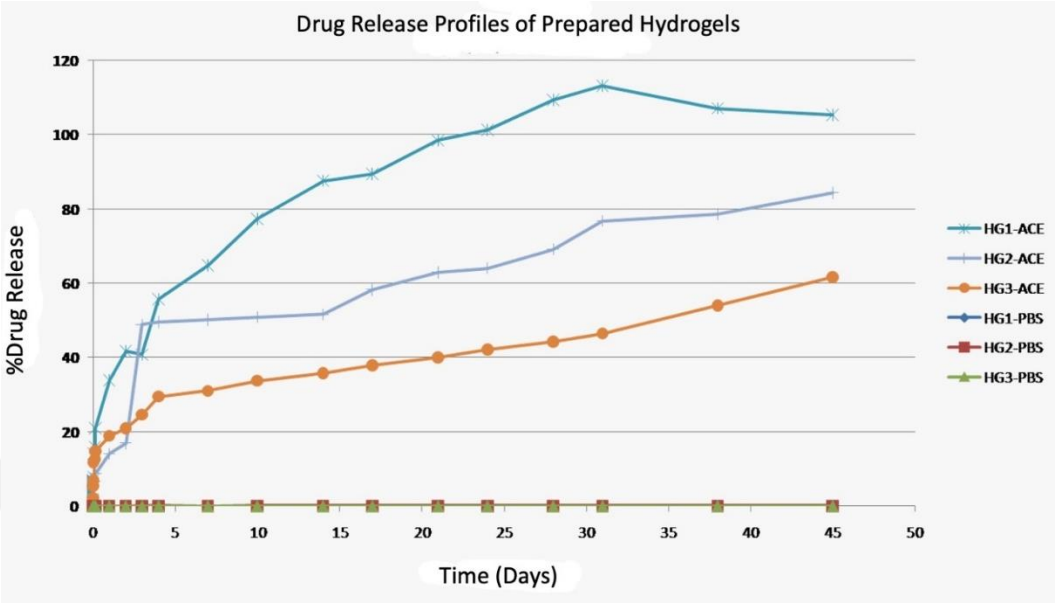

Figure 4.15. Drug release profile results based on percentage per day from prepared hydrogels

Table 4.4. Hydrogel scaffold encapsulation efficiency results

Hydrogel Groups	Ibu amount hydrogel (µg)	Ibu loaded amount (µg)	%Ibu Encapsulation Efficiency (%EE)
H1	2354.44	2500	94.1776
H2	4734.455	5000	94.6891
H3	7424.51	10000	74.2451

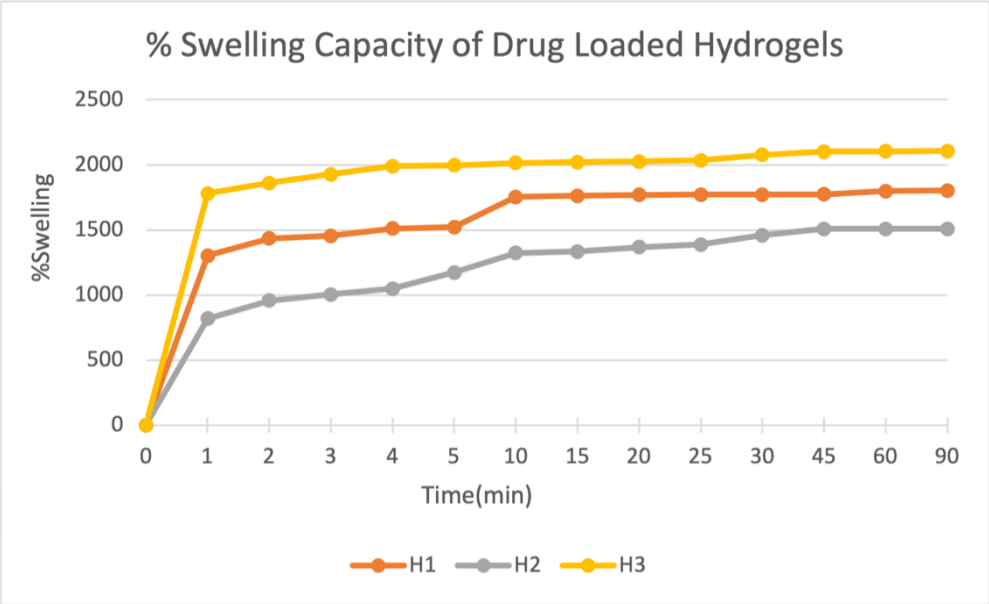

Figure 4.16. %Swelling capacity of drug loaded hydrogels

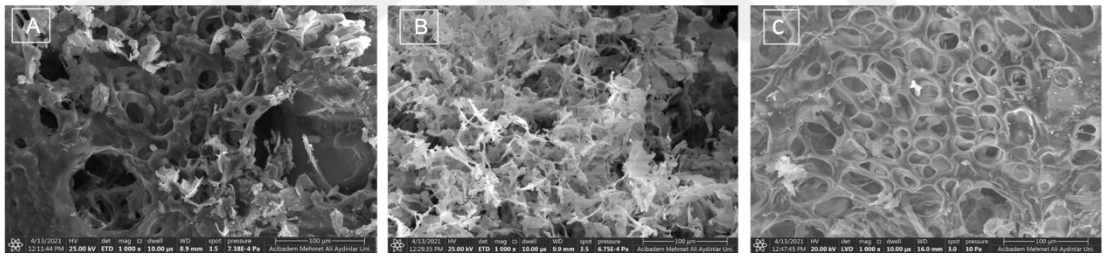

Figure 4.17. SEM images of drug loaded hydrogels A) H1 B) H2 C) H3

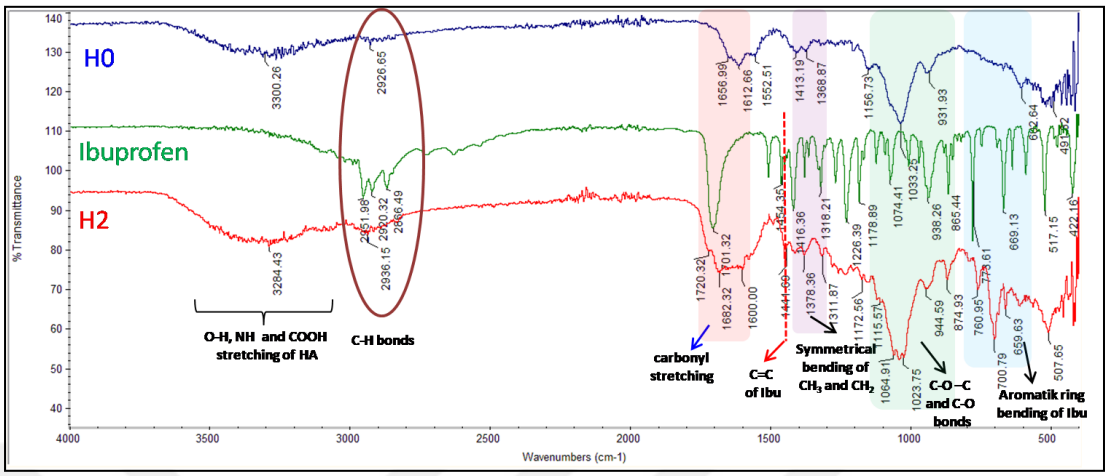

Figure 4.18. The FT-IR spectrum of the prepared drug-loaded hydrogel H2 and its comparison with the H0 and free drug spectra

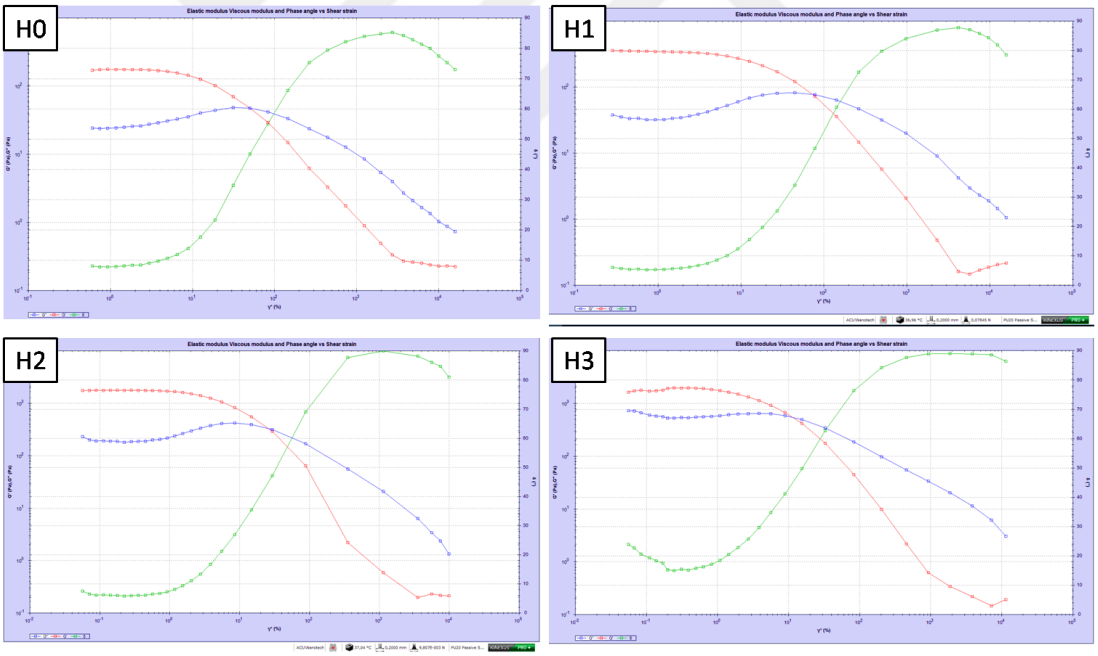

Figure 4.19. Rheometer analysis results of the prepared drug-loaded HA-MA hydrogels (3%)

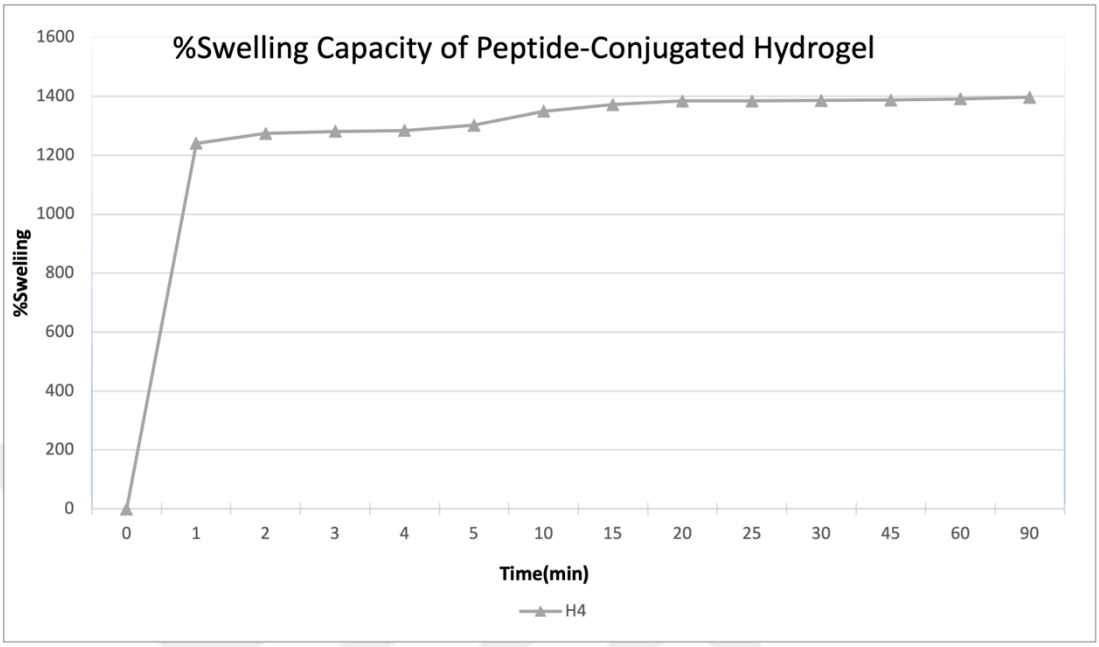

Figure 4.20. % Swelling capacity of peptide monomer conjugated hydrogel

Table 4.5. Results of peptide quantification assays of bioactive hydrogel H4

	% Peptide amount in hydrogel	**% Peptide immobilization efficiency**
BCA kit	0.381	38.1
Fluorometric peptide concentration kit	0.337	33.7

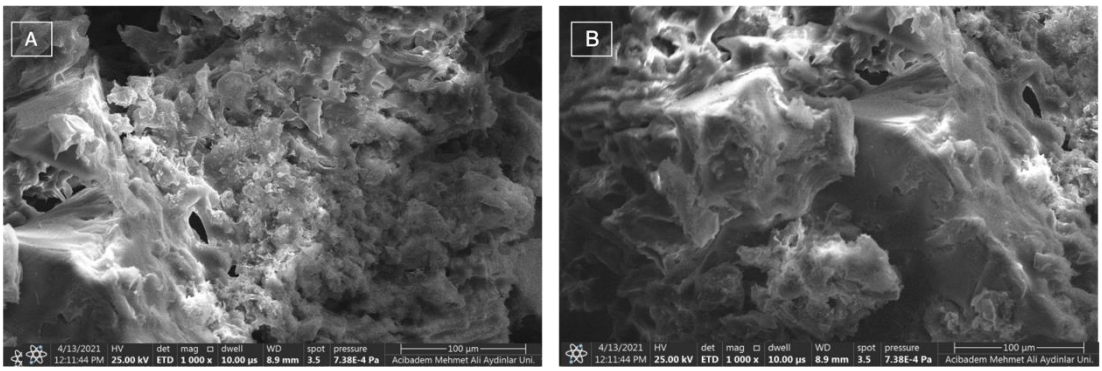

Figure 4.21. SEM images of peptide conjugated hydrogels A) 90-degree angle B) 45-degree angle

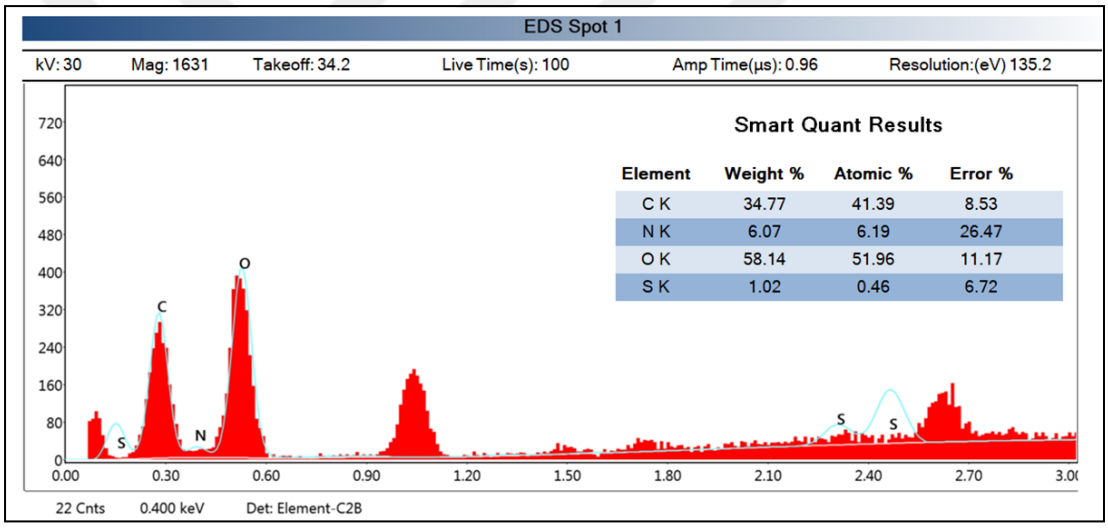

Figure 4.22. SEM-EDS analysis result of the prepared bioactive HA-MA hydrogel

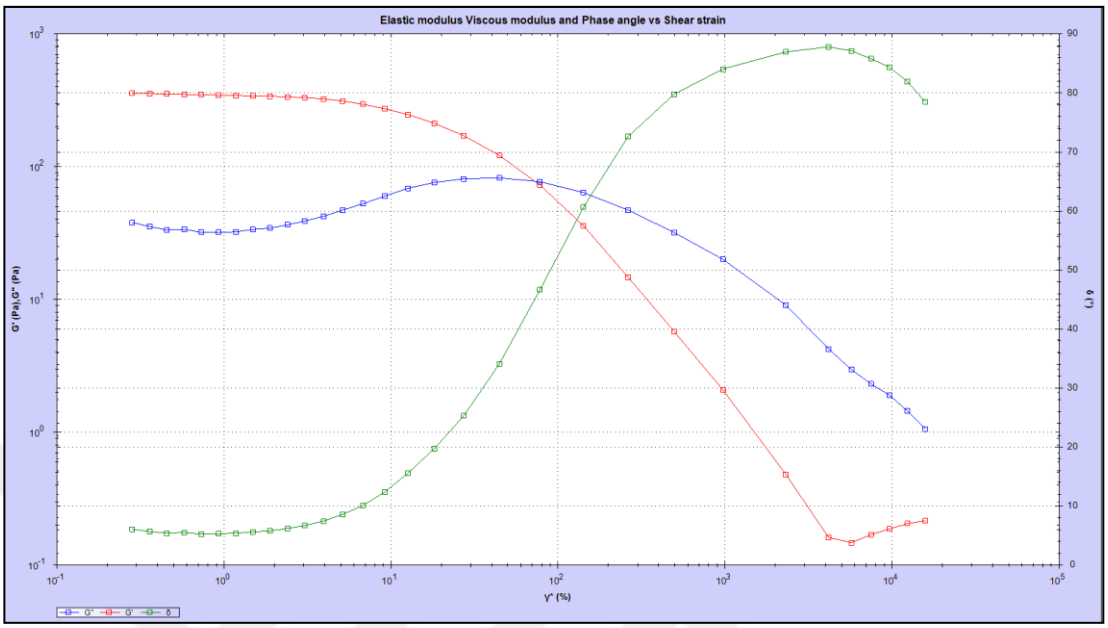

Figure 4.23. Rheometer analysis results of the peptide monomer conjugated HA-MA hydrogel (3%)

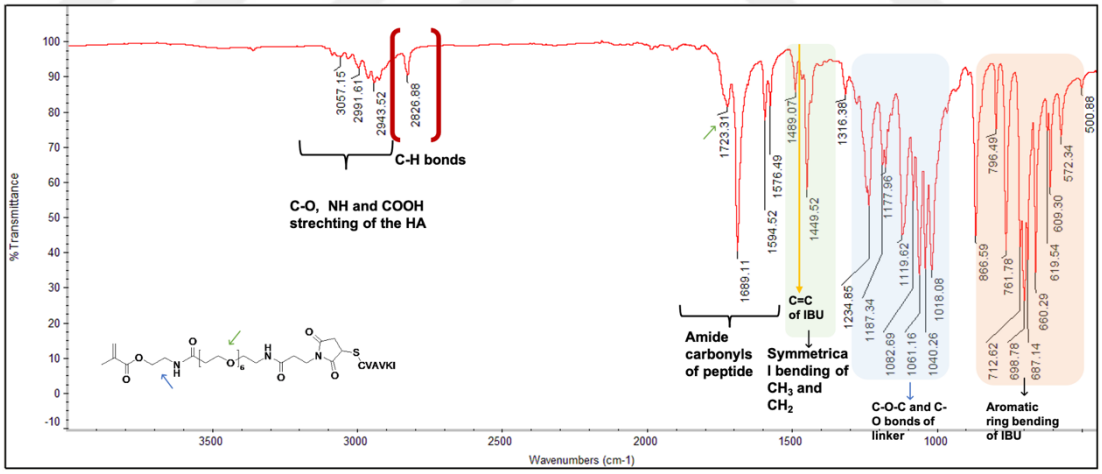

Figure 4.24. FT-IR analysis of IKVAV-MA conjugated hydrogel

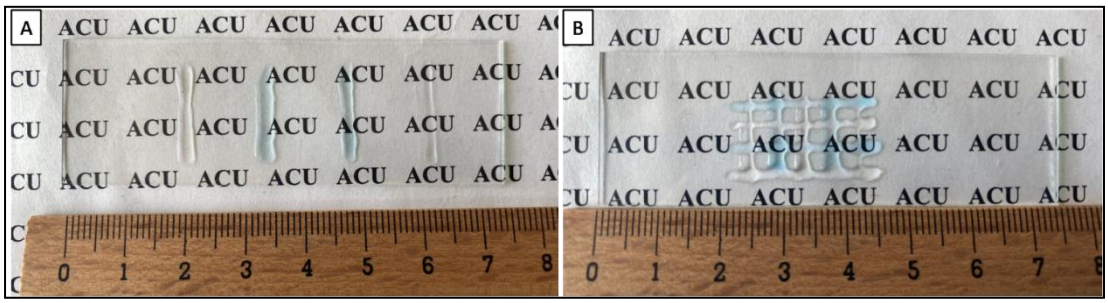

Figure 4.25. Hydrogel fibers printed with a 3D Bioprinter. A) 10mm line like structures printed B) Mesh like structure printed with dyed and non-dyed HA-MA

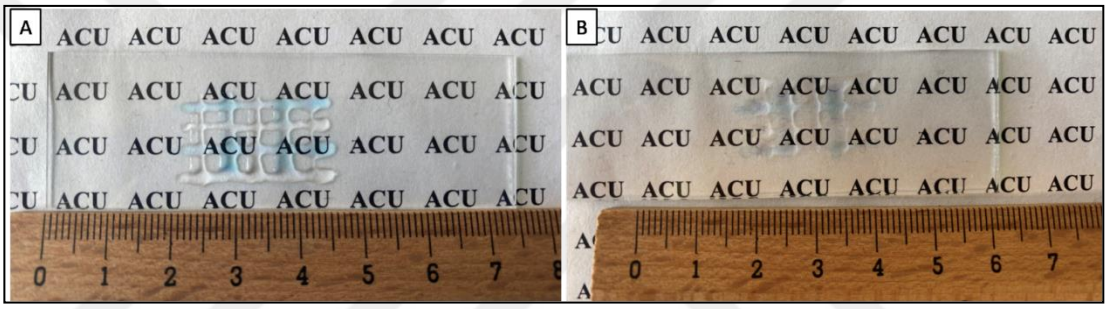

Figure 4.26. Hydrogel fibers printed with a 3D Bioprinter A) Before cross-linking B) After cross-linking

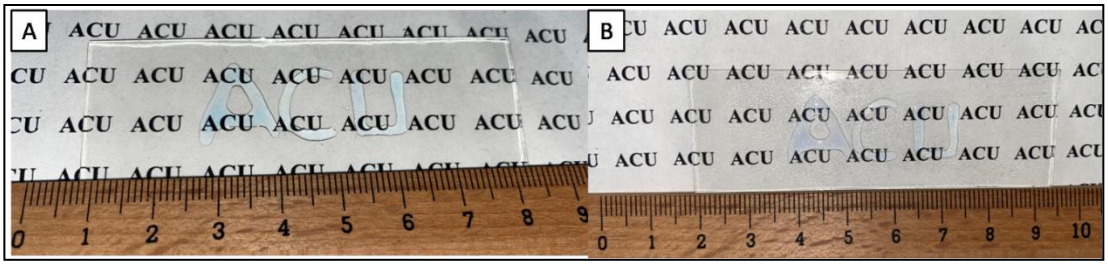

Figure 4.27. Hydrogel fibers printed with a 3D Bioprinter A) Before cross-linking B) After cross-linking

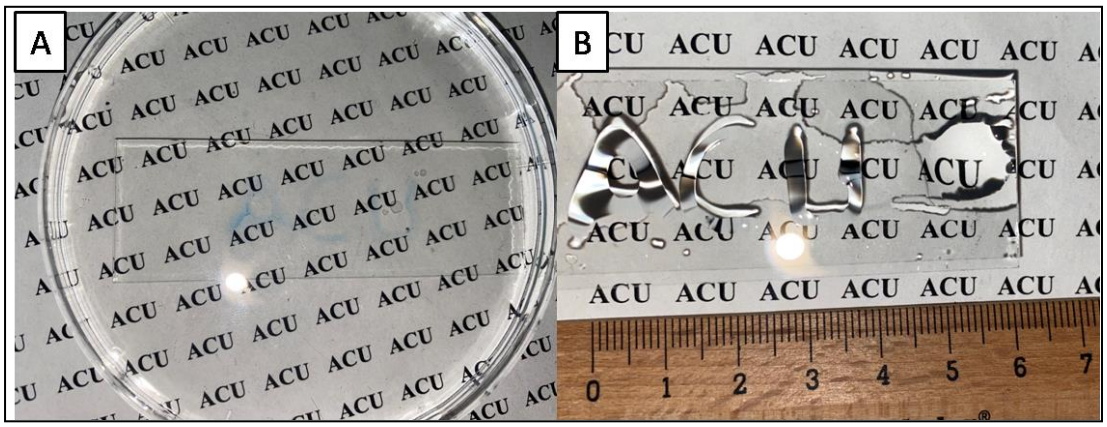

Figure 4.28. Pictures of hydrogel fibers printed with a 3D Bioprinter in water and after extraction

5. DISCUSSION

In order to show the presence of methylate groups in the chemical structure of HA-MA polymer, the peaks obtained in FT-IR spectroscopy were compared with the pure HA polymer peaks. As can be seen comparatively in Figure 4.1, the peaks seen at 1736 cm^{-1} frequency belong to the double bonds of the methacrylate functional groups attached to the side branches of the polymer chains. Again, the peaks representing the ester carbonyl group from the methacrylate group are seen around 1640 cm^{-1}, in a similar place with the amide and carboxylic acid peaks of the HA polymer. The characteristic O-H and COO-H bonds to the labile proton belonging to the HA polymer and the C-O symmetrical and asymmetrical stretching peaks are also seen in the HA-MA spectrum, with around 3300 and 1050 cm^{-1}, respectively (42).

The proton NMR spectrum of HA-MA polymer dissolved in DMSO and analyzed in 128 scans is shown in Figure 4.2. While the peak belonging to the solvent proton is seen at 2.50 ppm, the two peaks at 5.60 and 5.02 ppm belong to the protons ($H_2C=C$) in the methacrylate double bond. In addition, the $-CH_3$ peak, which represents the methyl group attached to the methacrylate group, is seen as a singlet at 1.78 ppm. The large and multiple peaks at 3.38 ppm represents the CH-O protons in the structure of the HA polymer.

In the chemical structure of the HA polymer, there is no proton that can be taken as a reference in the proton NMR spectrum; that is, since the whole polymer has similar protons and there is no chemical group with a defined number at the end or side branches of the polymer, it is quite difficult to determine the number of methacrylate groups attached per 1 HA chain by looking at the HNMR spectrum. Instead, it is possible to find a ratio by comparing the integration values of the peak representing the CH-O protons from the structure of the HA polymer and the peaks at 3.38 rpm belonging to the

methacrylate group (45). It is known that the HA polymer used is of medium molecular weight and its average molecular weight is ~$1.65x10^3$ kDa based on the literature. Considering that the monomers in the structure of this polymer have a molecular weight of approximately 170 Da, there are 9706 monomers in 1 HA chain. When the obtained analysis result is evaluated from this point of view and considering that there are 5 CH-O protons in a single monomer, the integration value of the CH-O peak in the HNMR spectrum is fixed to 9706x5=48530, and the integration of the peaks representing methacrylate is seen as 36. Since these peaks represent 1 methacrylate, the average number of methacrylate attached to the side branches of 1 HA chain can be calculated as 36. This ratio shows that HA-MA functional polymer containing 1.15 wt.% methacrylate can be obtained successfully.

Chemical characterization of the prepared HA-MA hydrogel was performed using FT-IR Spectroscopy. The hydrogel, which was also lyophilized and stored in a dry form, was analyzed with the FT-IR device by taking the air as a background. As seen in Figure 4.3, in this study, the wide peak observed at a frequency of around 3260 cm^{-1} belongs to the O-H, N-H and COO-H bonds in the HA structure. C-H aliphatic covalent bonds in the structure are represented by a peak around 2920 cm^{-1}. It is also possible to see the peaks of C-O and C-O-C bonds in the HA structure around 1050 cm^{-1}. While the two peaks seen at 1610 and 1550 cm^{-1} frequencies represent carbonyl groups in the amide and carboxylic acid groups in the HA structure, the peak around 1660 cm^{-1} clearly seen in the FT-IR spectrum of HA-MA belongs to the carbonyl bonds of the methacrylic ester groups in the structure. is considered (46).

In Figure 4.4, swelling capacity of HA-MA hydrogel was tested. The water holding capacity of hydrogels was high in the first minutes and increased by 200-300% relative to their dry weight. The hydrogels, which then absorbed more slowly, reached equilibrium after 10-15 minutes.

In Figure 4.5A-B, it is seen that the hydrogels have very smooth polymer walls, while the pores formed as a result of chemical cross-linking when dried by lyophilization are quite frequent and their size is micro-sized. It can be easily said that this pore size is suitable for the migration of surrounding tissue cells of this artificial tissue piece hydrogel structure, which is then desired to be implanted in the body.

The mechanical strength of this hydrogen structure was examined using a rheometer (Malvern, Kinexus) device. As seen in Figure 4.6, pure HA polymer (3%) was used, and the pH value of the medium was lowered (pH 5.5 acetate buffer solution). For the obtained hydrogel (A), there is little difference at the beginning of the analysis between the storage modulus G" representing the solid phase and the loss modulus G' representing the liquid phase. This pure HA hydrogel does not deform when the applied stress is increased, on the contrary, the G" value representing the solid phase gradually increases as the applied stress brings the polymer chains closer together. On the other hand, when the hydrogel obtained by using HA-MA polymer and curing under UV light is examined via rheometer and under the same conditions, it is seen that the difference between G" and G' modulus values is higher at the beginning of the analysis. First, this shows that the HA-MA (3%) hydrogel is stiffer than the hydrogel made with pure HA. As the amount of stress applied to this hydrogel is increased, it is seen that the storage modulus representing the solid phase for the hydrogel starts to decrease and the loss modulus representing the liquid phase increases. The intersection points can be considered as the point where deformation begins to be seen in the hydrogel, and this deformation increases as the stress increases. This can be considered as an indication that the obtained HA-MA hydrogel can react by being deformed according to the applied pressure and force and may be more responsive in the physiological environment.

UV-Vis Spectrophotometer calibration curve with PEGMA is used to prove methacrylate existence in both HA-MA1 (methacryloyl chloride and HA-MA2

(methacrylic anhydride). In Figure 4.7 and. Table 4.2, using PEGMA solutions as a control has proven that HA-MA1 and HA-MA2 is containing methacrylate in their chemical structure and their methacrylate concentrations does not differ significantly, respectively.

It was shown in Figure 4.8. chemical characterization of the prepared peptide monomer IKVAV-MA was performed using FT-IR Spectroscopy. This substance, which was lyophilized and stored dry, was analyzed with the FT-IR device by taking the air background. In this study, the wide peak observed at a frequency of around 3400-3200 cm^{-1} especially belongs to the O-H, N-H and COO-H bonds in the peptide structure. C-H aliphatic covalent bonds in the structure are represented by a peak around 2930 cm^{-1}. It is possible to see the peaks of C-O and C-O-C bonds in the short PEG chain structure of the intermediate linker molecule around 1100-1200 cm^{-1}. While the two peaks seen at 1647 and 1325 cm^{-1} frequencies represent the amide carbonyl groups in the structure of the peptide and intermittent molecule, the peak around 1702 cm^{-1}, which is clearly seen in the FT-IR spectrum of the HA-MA polymer, is thought to belong to the carbonyl bonds of the methacrylic ester groups in the structure (46).

It was shown that IKVAV-MA monomer, (Figure 4.9) whose purity level was checked using LC-MS (Thermo, DioNex Ultimate3000) device, was obtained with 82% purity. On the other hand, LC-MS/MS (Agilent, 1640) device was used to determine the molecular weight of the obtained monomer. C18 reversed phase column was used as stationary phase for both analyses. A mixture containing 50% ACN and 50% H2O was used as the mobile phase. Analyzes were performed at a flow rate of 0.5 mL/min and at 30 °C. In the LC-MS/MS analysis, along with the mass peak of the total molecular weight of the synthesized monomer, the peak of the +2 and 4 charged states are also seen in the positive scanning region.

It was shown that IKVAV-MA monomer, (Figure 4.10) whose purity level was checked using HPLC column chromatography with C18 column (Agilent VariTide RPC 250x10 mm ID). The column equilibrated by 5% mobile phase (B solution was Acetonitrile A solution was dH_2O containing 0,025% Trifluoracetic acid). Analyzes were performed at a flow rate of 0.5 mL/min and at 30 °C. Purity level was obtained as 86%.

Proton NMR Spectroscopy analysis was performed for the chemical structure determination of the synthesized peptide monomer. The analysis in dDMSO was performed in 64 scans and analyzed with the mestReNova program (Figure 4.11). In the obtained NMR spectrum, it is seen that two peaks at 5.25 and 5.67 ppm values belong to the methacrylate double bond protons in the structure. The singlet peak of the protons in the -CH3 group in the structure of the methacrylate group is seen at 1.25 ppm. The large wide peak seen around 3.5 ppm belongs to the CH2-O protons in the ethylene glycol-based polymer (PEG) structure in the structure of the intermediate linker molecule. With the peptide attached to the other end of the intermediate linker molecule, the d-marked proton in the maleimide ring came in at 6.1 ppm, as expected. It is seen that the mobile (labile) O-H, N-H and COO-H protons of the peptide come in the range of 7.3-8.5 ppm (47). In addition, amide carbonyl protons in the peptide structure can be seen around 3.65 ppm; and the methacrylic ester protons coming from the intermediate linker molecule in the structure are also seen in the range of 4.0-4.5 ppm. The peaks of aliphatic protons in the peptide structure were in the range of 0.7-2.2 ppm. Singlet peaks at 8.0 ppm and singlet peaks at 2.75 and 2.87 ppm are considered as DMF solvent peaks, which are thought to be left over from the synthesis step in this material. Therefore, both the protons of the methacrylate group, the monomer protons of the intermediate linker molecule, and the carbonyl and aliphatic protons of the peptide are seen in the HNMR spectrum of the prepared peptidic monomer, and the chemical structure of the IKVAV-MA monomer has been conformed.

UV-Vis spectrophotometer device was used to calculate the amount of drug loaded on these hydrogels. First, the free drug Ibuprofen was prepared at different concentrations and absorbance values were measured at the maximum wavelength of 264 nm (44), a calibration curve was drawn that relates these absorbance values to the concentration (Figure 4.12). After the drug-loaded hydrogels were prepared, washed, and removed from their impurities, the absorbances measurements were done by using UV-Vis spectrophotometer (Shimadzu, UV-2600) at 264 nm. The amount of drug in these solutions was determined by using the calibration curve drawn for the free drug. This value was compared with the amount of drug used initially while preparing the hydrogels, and the encapsulation efficiency was calculated separately for each hydrogel (Table 4.5).

For LC-MS/MS analysis, free drug molecules were analyzed in the first step. Ibuprofen solution was prepared at a concentration of 2500 ppb and given to the device at a flow of 0.5 mL/min for 1 minute with stationary phase C18 prep-HPLC column and mobile phase 50% ACN: 50% H2O. The mass peak and distribution of the free drug molecule in the MS2Scan scanning analysis is shown in Figure 4.13. The expected theoretical molecular weight of 206.13 $gmol^{-1}$ was found to be 263 $gmol^{-1}$ in mass analysis. This value indicates that the drug molecule may have formed a complex with formic acid used for ionization in the mobile phase medium. On the other hand, when the full molecular weight value is entered into the device in MS2SIM mode, it is seen in Figure 4.13 that the detector detects a peak of 205.0 $gmol^{-1}$ at high intensity as a result of the analysis. In addition, a peak of 177.1 $gmol^{-1}$, which has a higher intensity than the total molecular ion, is seen in the MS2Scan spectrum. Looking at the literature information, it can be seen that this value is the result of ibuprofen fragmentation. Therefore, when analyzing drug release samples, the method to be used for the quantification of free drug molecules in the medium was created according to the MRM mode, which goes from 263.1 $gmol^{-1}$ to 177.1 $gmol^{-1}$ (48).

After introducing ibuprofen to the LC-MS/MS device and creating a method suitable for this molecule, a calibration curve was drawn using this method in order to quantify it (41). For this, ibuprofen solutions at different concentrations were prepared by serial dilution method. These samples were analyzed using the method prepared from low to high concentration. Using the software of the device for quantitative analysis, a very reliable (R^2>0.992) calibration curve was drawn by matching the signals corresponding to these values with the concentration values of these solutions (Figure 4.14). This method and the calibration curve used to determine the amount of free drug in samples collected at different time points in drug release experiments (40).

After the drug release experiments, all collected samples were analyzed in the LC-MS/MS device using the above-mentioned method. The calibration curve of the free drug Ibuprofen was drawn using the software in this device, and then the files of the samples were evaluated on this curve. The concentration values that obtained were calculated as a percentage for each hydrogel based on the amount of drug which were initially encapsulated. For this purpose, the drug encapsulation efficiency percentages of each hydrogel given in Table 4.5 were evaluated according to the 5 mg hydrogel used in these drug release experiments, and the initial drug amounts in the 5 mg hydrogels were calculated. Then, with this LC-MS/MS analysis, a calculation was made as "What is the percentage of the initial drug amount for each time point in which the amount of free drug was calculated". Thus, for each hydrogel, % drug release profiles could be calculated and expressed graphically in Figure 4.15 in the same timeline.

The obtained drug loaded hydrogels (H1, 2 and 3) were investigated using the characterization methods specified in methods. First, the water holding capacity of the drug-containing gels was determined and compared with the control hydrogel, H0. As seen in Figure 4.16, the water holding capacity of drug-containing hydrogels was similarly high in the first minutes and increased by 200-300% relative to their dry weight. The

hydrogels, which then absorbed water more slowly, reached equilibrium after 10-15 minutes. It is thought that hydrogels which contains drugs have a structure that absorbs less water and reaches equilibrium more quickly than the control hydrogel, resulting from the hydrophobic nature of the encapsulated drug molecules (49).

The morphological structure of the prepared drug-loaded HA-MA hydrogel was made using Scanning Electron Microscopy (SEM-QuatroS). In Figure 4.17, it is observed that the drug-loaded hydrogels still have very smooth polymer walls while they can preserve their porous structure when dried by lyophilization with drug loading. When compared with the morphological features of the control hydrogel structure, it is observed that there are dot-shaped glows in the drug-loaded hydrogels' SEM images. It was observed that the irradiance and the whiteness of the images increased as the amount of drug loaded especially in the H1 and H2 hydrogels increased. This highlights the possibility that the hydrophobic drug molecules that are loaded can crystallize within the hydrophilic polymer network. It can be predicted that this situation may present a slower release profile in drug release profiles.

Chemical characterization of the prepared drug-encapsulated HA-MA hydrogels was performed using FT-IR Spectroscopy. The hydrogels, which were also lyophilized and stored dry, were analyzed with the FT-IR device by taking the air as a background. In Figure 4.18, the peak of the O-H, N-H and COO-H bonds in the HA structure is observed at a frequency of around 3300 cm^{-1}. C-H aliphatic covalent bonds in both polymers and drug molecules are represented by multiple peaks around 2920 cm^{-1}. It is also possible to see the peaks of C-O and C-O-C bonds in the HA structure around 1040 cm^{-1}. While the two peaks at 1610 and 1550 cm^{-1} frequencies represent the carbonyl groups in the amide and carboxylic acid groups in the HA structure, the carboxylic acid peak from the Ibuprofen structure is also seen in the H2 spectrum as a sharp peak at 1720 cm^{-1} frequency. Again, the C=C stretching peak of the aromatic right in the structure of Ibuprofen is around

1450 cm^{-1}; bending peaks are also seen in a multiple pattern at the expected frequency of 900-700 cm^{-1} (50).

The mechanical strength of the obtained drug-loaded hydrogels was investigated using a rheometer device. The method and device parameters specified in methods were also used in this study (43). Deformation levels against applied stress were measured for hydrogels H1, H2 and H3, which were prepared at the same concentration as the control hydrogel H0, and with increasing drug amount, using a rheometer device. As seen in the control hydrogel, there is a similar difference between the storage modulus G" representing the solid phase and the loss modulus G' representing the liquid phase at the starting point in drug-loaded hydrogels. As the amount of stress applied to these hydrogels is increased, it is seen that the storage modulus representing the solid phase for the hydrogel starts to decrease and the loss modulus representing the liquid phase increases. The intersection points can be considered as the point where deformation begins to be seen in the hydrogel, and this deformation increases as the stress increases. In addition, as the amount of stress applied to the hydrogels increased, it was observed that the deformation of the hydrogels had a similar pattern to the control hydrogel and did not generally change the effect of drug loading on gel stiffness and hardness (Figure 4.19).

Peptide immobilization step was carried out by using the H2 hydrogel, which has the best values in terms of %EE and amount of drug from these synthesized drug-loaded hydrogels. For this, all the components in the structure of the H2 hydrogel were added into the vial in the same way (amount and concentration). Then, IKVAV-MA peptide monomer was weighed and added at 1% by weight relative to the total amount of polymer. This peptide mixture was gelled by curing under the same conditions, i.e., for 3 hours and under UV light (365 nm). This hydrogel obtained was numbered H4 and was washed with distilled water at least 3 times to remove impurities and unencapsulated drug molecules. In this study, the HA-MA methacrylate reacted radically while gelating through the

methacrylate group in the structure of the IKVAV-MA molecule, which is a peptide monomer, and thus the IKVAV peptide was attached to the hydrogel structure formed by covalent bonds. The results of characterization studies of this obtained hydrogel together with other drug-loaded hydrogels are described in methods.

In Figure 4.20, similarly, the water holding capacity of the peptide immobilized hydrogels increased significantly in the first minutes and increased by 500-600% relative to their dry weight. The hydrogels, which then absorbed more slowly, reached equilibrium after 10-15 minutes. It is thought that the hydrogels containing the peptide monomer have a structure that absorbs less water and reaches equilibrium more quickly than the control hydrogel, due to the hydrophobic nature of the peptide monomer.

Two different measurement methods were tried to determine the amount of peptide molecule in the peptide immobilized hydrogels prepared. The first method for the peptide quantitation experiment conducted by using the Pierce™ BCA Protein Kit (Thermo ScientificTM). By using this kit, it is possible to measure the amount of protein in the solution with a spectrophotometric method. It is known that this method is also used in the quantitation of peptide sequences that are smaller than proteins. The reagent used in this method turns into a chromogenic complex in the presence of protein and the absorbance value obtained using a UV-Vis spectrophotometer (Shimadzu, UV-2600) at 562 nm was correlated with the amount of protein using the appropriate calibration curve (51). The other method is based on the use of the commercially purchased PierceTM Quantitative Fluorometric Peptide Kit (Thermo ScientificTM) (52). In this method, a fluorometric complex is formed as a result of the interaction of a reactive molecule in the kit with specifically peptide molecules in the solution, and the fluorescent signal of this complex was measured using a Thermo Scientific Varioskan Flash plate reader. Table 4.6 shows the results of the analyses made with both measurement methods. According to these results, 35% of the peptide molecules added to the medium while preparing the H4

hydrogel is added to the hydrogel structure.

In the morphological analyzes performed for the H4 scaffold, which is a peptide-loaded hydrogel, smooth polymer walls are also seen in the SEM image of the hydrogel. (Figure 4.21) On the other hand, in the SEM image of the hydrogel (both the porous structure is clearly and neatly seen, and the encapsulated peptide molecules are evident by making whiter radiation compared to the HA polymer wall, as in the SEM images of other drug-loaded hydrogels.

In order to prove the existence of peptide molecules integrated into the hydrogel structure, atomic diagnosis and semi-quantitative atomic weight analyzes were performed using the EDS detector connected to the SEM microscope (53). Figure 4.22 shows the result of the EDS analysis. The S (Sulphur) atom seen in the hydrogel structure indicates the presence of the IKVAVC peptide, which has been end-modified with the cysteine amino acid and thus bound to the maleimide group in the intermediate linker molecule and turned into a monomer.

The mechanical strength of the obtained drug-loaded hydrogels was investigated using a rheometer device. The method and device parameters specified in methods were also used in this study (43). Deformation levels against applied stress were measured for hydrogel H4, which were prepared at the same concentration as the control hydrogel H0, and with the same amount of drug as hydrogel H2, using a rheometer device. As the amount of stress applied to these hydrogels is increased, it is seen that the storage modulus representing the solid phase for the hydrogel starts to decrease and the loss modulus representing the liquid phase increases. The intersection points can be considered as the point where deformation begins to be seen in the hydrogel, and this deformation increases as the stress increases. In addition, as the amount of stress applied to the hydrogels

increased, it was observed that the deformation of the hydrogel had a similar pattern to the control hydrogels seen in Figure 4.2 and did not generally change the effect of drug and peptide loading on gel stiffness and hardness.

Chemical characterization of the prepared HA-MA hydrogel was performed using FT-IR Spectroscopy. The hydrogel, which was also lyophilized and stored in a dry form, was analyzed with the FT-IR device by taking the air as a background. As seen in Figure 4.24, in this study, the wide peak observed at a frequency of around 3057 cm^{-1} belongs to the O-H, N-H and COO-H bonds in the in the peptide structure. C-H aliphatic covalent bonds in the structure are represented by a peak around 2940 cm^{-1}. It is also possible to see the peaks of C-O and C-O-C bonds in the HA structure around 1050 cm^{-1}. It is possible to see the peaks of C-O and C-O-C bonds in the short PEG chain structure of the intermediate linker molecule around 1100-1200 cm^{-1}. While the two peaks seen at 1647 and 1325 cm^{-1} frequencies represent the amide carbonyl groups in the structure of the peptide and intermittent molecule, the peak around 1720 cm^{-1}, which is clearly seen in the FT-IR spectrum of the HA-MA polymer, is thought to belong to the carbonyl bonds of the methacrylic ester groups in the structure.

The carboxylic acid peak from the Ibuprofen structure is also seen in the spectrum as a sharp peak at 1720 cm^{-1} frequency. Again, the C=C stretching peak of the aromatic right in the structure of Ibuprofen is around 1450 cm^{-1}; bending peaks are also seen in a multiple pattern at the expected frequency of 870-700 cm^{-1} (50). It is possible to see the peaks of C-O and C-O-C bonds in the short PEG chain structure of the intermediate linker molecule around 1100-1200 cm^{-1}.

For the peptide immobilized hydrogels prepared within the scope of the project to contribute to nerve tissue regeneration, besides the immobilization of IKVAV peptide

sequences to the hydrogel structure, it is aimed to add this peptide to this artificial tissue candidate hydrogel directionally. For this purpose, 3D printing technique was used (23). Then, the printed structures on a slide were placed in distilled water and left for 1 minute to see if these polymeric fibers exposed to UV light were truly crosslinked. On the slide removed from the water, the fibers are still clearly visible and discrete (Figure 4.28).

In Figure 4.27, the polymeric fiber ACU printed before exposure to UV light (A) is shown as the inscription. It is seen that these fibers have a very smooth structure and can remain without intermingling and dispersion. These polymeric fibers were then UV cured for 20 minutes and the image in Figure 4.27B was obtained. It is also seen that a smooth and well-preserved structure can be obtained.

The printed structures were placed in distilled water and left for 1 minute to determine whether these obtained fibers were indeed crosslinked by UV curing. Then, after it was lifted and excess water was removed, the image in Figure 4.28B was obtained. Thus, after UV curing, it was shown that polymers and peptidic monomer, can form fiber-shaped hydrogels.

6. CONCLUSION

According to the results obtained after all the characterization steps, it was decided that the H2 (Table 3.1) hydrogel had optimum properties since its water holding capacity is similar to the H0 (HA-MA) (Hydrogel containing only 3% Hyaluronic Acid methacrylate) hydrogel. Also, in terms of the structure's stability and rigidity, the rheological experiments showed that the scaffold is not affected by drug loading. The functional group analysis proved that H2 encapsulated the drug. Also, drug release profile showed that H2 hydrogel releases the loaded drug molecules slower than the other hydrogel structures, which can be suitable for promoting nerve regeneration in damaged tissues. Since H2 shows the characteristics of a hydrogel scaffold such as the smoothness of the polymer wall and a porous structure, H2 hydrogels prepared were used to obtain peptide-linked hydrogels, which was abbreviated as H4. Based on the FT-IR spectra, EDS data, BCA and Fluorometric Assays of the prepared gels, it was proven that the H4 hydrogel involves the loaded and desired peptide monomer.

The hydrogels prepared in this project are designed to support nerve cell adhesion. The IKVAV peptide which improves cell adhesion in general, is immobilized to 3-dimensional scaffolds with chemical bonds. The structure of prepared bioactive hydrogels has been tried to be adjusted so that the mechanical properties of the natural nervous tissue can be mimicked. The water holding capacity of bioactive hydrogels was high because of hyaluronic acid and the durability of the scaffold was increased with UV crosslinking via DMPA. Although, cross-linked hydrogels from hyaluronic acid are slowly biodegradable in the body, it was proven in this thesis that they can be deformed at high pressure with rheological data. The hydrogels have been prepared in order to have a long-term effect.

It has been shown that the hydrogel structures with these results, which are supported by the SEM images, have a morphological structure that can be suitable for the passage and migration behavior of the neural cells.

The aim of this project, the preparation of a biomaterial platform that can be used as the main scaffold in disease associated nerve tissue damage, has been successfully accomplished. The data obtained and the experience gained in this project will lead to the preparation of larger scale and disease specific scaffolds.

7. REFERENCES

1. Berthiaume F, Maguire TJ, Yarmush ML. Tissue engineering and regenerative medicine: History, progress, and challenges. Annu Rev Chem Biomol Eng. 2011;2:403–30.

2. Lee KY, Mooney DJ. Hydrogels for tissue engineering. Chem Rev. 2001;101(7):1869–79.

3. Fokunang CN, Ndikum V, Tabi OY, Jiofack RB, Ngameni B, Guedje NM, et al. Traditional medicine: Past, present and future research and development prospects and integration in the national health system of Cameroon. African J Tradit Complement Altern Med. 2011;8(3):284–95.

4. Hasan A. Tissue Engineering for Artificial Organs. Tissue Eng Artif Organs Regen Med Smart Diagnostics Pers Med [Internet]. 2017;1–2:1–34. Available from: http://doi.wiley.com/10.1002/9783527689934

5. Marti ME, Sharma AD, Sakaguchi DS, Mallapragada SK. Nanomaterials for neural tissue engineering [Internet]. Nanomaterials in Tissue Engineering: Fabrication and Applications. Woodhead Publishing Limited; 2013. 275–301 p. Available from: http://dx.doi.org/10.1533/9780857097231.2.275

6. Verreck G, Chun I, Li Y, Kataria R, Zhang Q, Rosenblatt J, et al. Preparation and physicochemical characterization of biodegradable nerve guides containing the nerve growth agent sabeluzole. Biomaterials. 2005;26(11):1307–15.

7. Haile Y, Haastert K, Cesnulevicius K, Stummeyer K, Timmer M, Berski S, et al. Culturing of glial and neuronal cells on polysialic acid. Biomaterials. 2007;28(6):1163–73.

8. Chen PR, Chen MH, Lin FH, Su WY. Release characteristics and bioactivity of gelatin-tricalcium phosphate membranes covalently immobilized with nerve growth factors. Biomaterials. 2005;26(33):6579–87.

9. Mitra J, Tripathi G, Sharma A, Basu B. Scaffolds for bone tissue engineering: Role of surface patterning on osteoblast response. RSC Adv. 2013;3(28):11073–94.

10. Wen X, Saijilafu, Luo Z, Yang H, Wang W, Yang L. Biomaterials and scaffolds for the treatment of spinal cord injury [Internet]. Biomaterials in Translational Medicine: A Biomaterials Approach. Elsevier Inc.; 2018. 117–139 p. Available from: http://dx.doi.org/10.1016/B978-0-12-813477-1.00006-2

11. Ahmed EM. Hydrogel: Preparation, characterization, and applications: A review. Vol. 6, Journal of Advanced Research. 2015. p. 105–21.

12. P. SS, Ajeet G, Shilpa B, Pankaj G. Hydrogels : Introduction , Preparation , Characterization and Applications. Int J Res Methodol. 2015;1(1):47–71.

13. Kamath KR, Park K. Biodegradable hydrogels in drug delivery. Adv Drug Deliv Rev. 1993;11(1–2):59–84.

14. Wagner A. Synthesis and Characterization of Hyaluronic Acid Based Biomaterials for Drug Delivery and Virus Modification. 2019;

15. Prehm P. Hyaluronate is synthesized at plasma membranes. Biochem J. 1984;220(2):597–600.

16. Chen WYJ, Abatangelo G. Functions of hyaluronan in wound repair. Wound Repair Regen. 1999;7(2):79–89.

17. Neuman MG, Nanau RM, Oruña-Sanchez L, Coto G. Hyaluronic acid and wound healing. J Pharm Pharm Sci. 2015;18(1):53–60.

18. Krishnakumar GS, Sampath S, Muthusamy S, John MA. Importance of crosslinking strategies in designing smart biomaterials for bone tissue engineering: A systematic review. Mater Sci Eng C [Internet]. 2019;96(December 2018):941–54. Available from: https://doi.org/10.1016/j.msec.2018.11.081

19. Qiu Y, Park K. Environment-sensitive hydrogels for drug delivery. Adv Drug Deliv Rev. 2001;53(3):321–339.

20. Kubyshkina G, Zupan B, Štukelj M, Grošelj D, Marion L, Emri I. The Influence of Different Sterilization Techniques on the Time-Dependent Behavior of Polyamides. 2011;2011(October):361–8.

21. Boelen EJH, Koole LH, van Rhijn LW, van Hooy-Corstjens CSJ. Towards a functional radiopaque hydrogel for nucleus pulposus replacement. J Biomed Mater Res [Internet]. 2007;Part B, Ap(2):440–50. Available from: https://proxy.library.upenn.edu/login?url=http://ovidsp.ovid.com/ovidweb.cgi?T=JS&CSC=Y&NEWS=N&PAGE=fulltext&D=med4&AN=17415776%5Cnhttp://elinks.library.upenn.edu/sfx_local?sid=OVID:medline&id=pmid:17415776

22. Photocrosslinkable Hydrogels for 3D Cell Culture and Tissue Engineering [Internet]. Available from: https://www.sigmaaldrich.com/NL/en/technical-documents/technical-article/cell-culture-and-cell-culture-analysis/3d-cell-culture/photocrosslinked-hydrogels

23. Poldervaart MT, Goversen B, De Ruijter M, Abbadessa A, Melchels FPW, Öner FC, et al. 3D bioprinting of methacrylated hyaluronic acid (MeHA) hydrogel with intrinsic osteogenicity. PLoS One. 2017;12(6):1–15.

24. Kim J, In SK, Soon JH, Ho CK, Park Y, Sun K. Bone regeneration using MMP sensitive-hyaluronic acid based hydro gels. Bioeng Proc Northeast Conf. 2009;7–8.

25. Sohdi AA, Campbell D, Topham PD. Polymer-Peptide Conjugate Hydrogels; Towards Controlled Drug Delivery. Chiang Mai J Sci. 2012;39(3):351–72.

26. Sun Y, Li W, Wu X, Zhang N, Zhang Y, Ouyang S, et al. Functional Self-Assembling Peptide Nanofiber Hydrogels Designed for Nerve Degeneration. ACS Appl Mater Interfaces. 2016;8(3):2348–59.

27. Gelain F, Bottai D, Vescovi A, Zhang S. Designer self-assembling peptide nanofiber scaffolds for adult mouse neural stem cell 3-dimensional cultures. PLoS One. 2006;1(1).

28. Hou S, Tian W, Xu Q, Cui F, Zhang J, Lu Q, et al. The enhancement of cell adherence and inducement of neurite outgrowth of dorsal root ganglia co-cultured with hyaluronic acid hydrogels modified with Nogo-66 receptor antagonist in vitro. Neuroscience. 2006;137(2):519–29.

29. Lin CM, Lin JW, Chen YC, Shen HH, Wei L, Yeh YS, et al. Hyaluronic acid inhibits the glial scar formation after brain damage with tissue loss in rats. Surg Neurol [Internet]. 2009;72(SUPPL. 2):S50–4. Available from: http://dx.doi.org/10.1016/j.wneu.2009.09.004

30. Özgenel GY. Effects of hyaluronic acid on peripheral nerve scarring and regeneration in rats. Microsurgery. 2003;23(6):575–81.

31. Khaing ZZ, Milman BD, Vanscoy JE, Seidlits SK, Grill RJ, Schmidt CE. High molecular weight hyaluronic acid limits astrocyte activation and scar formation after spinal cord injury. J Neural Eng. 2011;8(4).

32. Jensen G, Holloway JL, Stabenfeldt SE. Hyaluronic Acid Biomaterials for Central Nervous System Regenerative Medicine. Cells. 2020;9(9):1–17.

33. Spearman BS, Agrawal NK, Rubiano A, Simmons CS, Mobini S, Schmidt CE. Tunable methacrylated hyaluronic acid-based hydrogels as scaffolds for soft tissue engineering applications. J Biomed Mater Res - Part A. 2020;108(2):279–91.

34. Oudshoorn MHM, Rissmann R, Bouwstra JA, Hennink WE. Synthesis of methacrylated

hyaluronic acid with tailored degree of substitution. Polymer (Guildf). 2007;48(7):1915–20.

35. Burdick JA, Prestwich GD. Hyaluronic acid hydrogels for biomedical applications. Adv Mater. 2011;23(12):41–56.

36. Smeds KA, Grinstaff MW. No Title. Dep Chem Ophthalmol. 2000;54(1):115–21.

37. Leach JB, Bivens KA, Patrick CW, Schmidt CE. Photocrosslinked hyaluronic acid hydrogels: Natural, biodegradable tissue engineering scaffolds. Biotechnol Bioeng. 2003;

38. Prata JE, Barth TA, Bencherif SA, Washburn NR. Complex fluids based on methacrylated hyaluronic acid. Biomacromolecules. 2010;11(3):769–75.

39. Xiao SJ, Brunner S, Wieland M. Reactions of surface amines with heterobifunctional cross-linkers bearing both succinimidyl ester and maleimide for grafting biomolecules. J Phys Chem B. 2004;

40. Zarzycki R, Modrzejewska Z, Nawrotek K, Leków U, Hydrożeli Z. Drug Release from Hydrogel Matrices. Ecol Chem Eng Sci. 2010;

41. Papageorgiou S, Varvaresou A, Panderi I, Giannakou M, Spiliopoulou C, Athanaselis S. Development and validation of a reversed-phase high-performance liquid chromatographic method for the quantitation and stability of α-lipoic acid in cosmetic creams. Int J Cosmet Sci. 2020;

42. Lim HJ, Perera TH, Wilems TS, Ghosh S, Zheng YY, Azhdarinia A, et al. Response to di-functionalized hyaluronic acid with orthogonal chemistry grafting at independent modification sites in rodent models of neural differentiation and spinal cord injury. J Mater Chem B. 2016;

43. Karvinen J, Ihalainen TO, Calejo MT, Jönkkäri I, Kellomäki M. Characterization of the microstructure of hydrazone crosslinked polysaccharide-based hydrogels through rheological and diffusion studies. Mater Sci Eng C. 2019;

44. On a R, Targeting D, Carriers D. in Pharmaceutical and Nano Sciences. 2013;2(6):478–84.

45. Vasi AM, Popa MI, Butnaru M, Dodi G, Verestiuc L. Chemical functionalization of hyaluronic acid for drug delivery applications. Mater Sci Eng C. 2014;

46. Li X, Lian C, Zhi D, Xu S, Liu H. Synthesis and swelling behavior of SiO2-HA/PNIPAm core-shell structured thermoresponsive microgels. Acta Chim Sin. 2014;

47. BOGUSKY MJ, NAYLOR AM, PITZENBERGER SM, NUTT RF, BRADY SF, COLTON CD, et al. NMR and molecular modeling characterization of RGD containing peptides. Int J Pept Protein Res. 1992;

48. Puangpetch A, Limrungsikul A, Prommas S, Rukthong P, Sukasem C. Development and validation of a liquid chromatography-tandem mass spectrometry method for determination of ibuprofen in human plasma. Clin Mass Spectrom. 2020;

49. Weeks A, Morrison D, Alauzun JG, Brook MA, Jones L, Sheardown H. Photocrosslinkable hyaluronic acid as an internal wetting agent in model conventional and silicone hydrogel contact lenses. J Biomed Mater Res - Part A. 2012;

50. Arslan H, Sahin NÖ. Characterization of ibuprofen solid dispersion part-II: FT-IR and DFT studies. Asian J Chem. 2007;

51. Olson BJSC, Markwell J. Assays for Determination of Protein Concentration. Curr Protoc Pharmacol. 2007;

52. Espadas G, Borràs E, Chiva C, Sabidó E. Evaluation of different peptide fragmentation types and mass analyzers in data-dependent methods using an Orbitrap Fusion Lumos Tribrid mass spectrometer. Proteomics. 2017;

53. Akdemir ZS, Akçakaya H, Kahraman MV, Ceyhan T, Kayaman-Apohan N, Güngör A. Photopolymerized injectable RGD-modified fumarated poly(ethylene glycol) diglycidyl ether hydrogels for cell growth. Macromol Biosci. 2008;

8. APPENDICES

Appendix 1: Hydrogel characterization

Time (min)	H0	H1	H2	H3	H0 with 1% peptide
0	6,8	5,5	5,5	5,8	5,7
1	61,4	77,2	50,5	109	76,4
2	67,2	84,4	58,2	113,7	78,3
3	67,4	85,5	60,7	117,6	78,7
4	73,2	88,6	63,2	121,2	78,9
5	78	89,2	70,1	121,6	79,9
10	78,9	102	78,3	122,6	82,6
15	79,9	102,4	78,9	123,1	83,9
20	80	102,8	80,7	123,3	84,6
25	83,9	102,9	81,8	123,8	84,6
30	84,6	102,9	85,8	126,3	84,7
45	84,6	103	88,4	127,7	84,8
60	84,7	104,4	88,5	127,8	85
90	84,8	104,6	88,5	128	85,3
	(mg)	(mg)	(mg)	(mg)	(mg)

Figure 8.1. Raw data of %Swelling Capacities of hydrogel structures

Gel Groups	HA-MA Dry Gel Weights mg	Initiator dry weight mg	Drug dry weight mg	Drug Loaded HA-MA crosslinked dry weight mg
H0 -no drug	77,4	30	0	83,8
H1	56	30	15	56,5
H2	43	30	30	31,8
H3	56,3	30	60	54,3
			IKVAVC monomer	
H4-Peptide	55,4	30	3	62,7

Figure 8.2. Raw data of Gel conversion rates

Appendix 2: Drug release studies

Standard Table

	Sample ID	Type	Ex	Conc	WL208,0	Wgt.Factor	Comments
1	PEGMA10	Standard		0.009	0.312	1.000	
2	PEGMA9	Standard		0.018	0.621	1.000	
3	PEGMA8	Standard		0.036	1.224	1.000	
4	PEGMA7	Standard		0.078	2.366	1.000	
5	PEGMA6	Standard		0.156	3.326	1.000	
6	PEGMA5	Standard		0.313	3.444	1.000	
7	PEGMA4	Standard		0.625	3.547	1.000	
8	PEGMA3	Standard		1.250	3.662	1.000	
9	PEGMA2	Standard		2.500	3.769	1.000	
10	PEGMA1	Standard		5.000	3.884	1.000	
11	PEGMA0	Standard		10.000	4.031	1.000	
12	PEGMA_1	Standard	✓	20.000	4.223	1.000	
13	PEGMA_2	Standard		7.500	3.982	1.000	
14							

Figure 8.3. Raw data of PEGMA standard curve in PBS

Standard Table

	Sample ID	Type	Ex	Conc	WL264	Wgt.Factor	Comments
1	IBU8	Standard		0.007	-0.006	1.000	50%AcN
2	IBU7	Standard		0.016	0.014	1.000	
3	IBU6	Standard		0.031	0.047	1.000	
4	IBU5	Standard		0.063	0.102	1.000	
5	IBU4	Standard		0.125	0.202	1.000	
6	IBU3	Standard		0.250	0.420	1.000	
7	IBU2	Standard		0.500	0.964	1.000	
8	IBU1	Standard		1.000	1.723	1.000	
9							

Figure 8.4 Raw data of Ibuprofen standard curve in 50% ACN

T0	Start point	Date
T1	15mins	15.03.2021
T2	30 mins	15.03.2021
T3	45 mins	15.03.2021
T4	1 hour	15.03.2021
T5	2 hours	15.03.2021
T6	3 hours	15.03.2021
T7	4 hours	15.03.2021
T8	24 hours	16.03.2021
T9	48 hours	17.03.2021
T10	72 hours	18.03.2021
T11	96 hours- 4th day	19.03.2021
T12	7th day	22.03.2021
T13	10th day	25.03.2021
T14	14th day	29.03.2021
T15	17th day	1.04.2021
T16	21st day	5.04.2021
T17	24th day	8.04.2021
T18	28th day	12.04.2021
T19	31st day	15.04.2021
T20	38th day	22.04.2021
T21	45th day	29.04.2021

Figure 8.5 Raw data of Time points which drug release samples were taken

9. CURRICULUM VITAE

Personal Information

Name		**Surname**	
Place of Birth		**Date of Birth**	
Nationality		**Telephone Number**	
E-mail			

Education

	Institution Name	**Graduation Year**
Master of Science		
Undergraduate		
High School		

Work Experience

Position	Corporation	Duration

Foreign Language

Language	Reading*	Speaking-	Writing*

***** Evaluated as advanced, good,intermediate,beginner

Foreign Language Exam Results#

KPSS	ÜDS	IELTS	TOEFL IBT	TOEFL PBT	TOEFL CBT	OTHER

KPDS: Kamu Personeli Yabancı Dil Sınavı; ÜDS: Üniversitelerarası Kurul Yabancı Dil Sınavı; IELTS: International English Language Testing System; TOEFL IBT: Test of English as a Foreign Language-Internet-Based Test TOEFL PBT: Test of English as a Foreign Language-Paper-Based Test; TOEFL CBT: Test of English as a Foreign Language-Computer- Based Test; FCE: First Certificate in English; CAE: Certificate in Advanced English; CPE: Certificate of Proficiency in English

Other Exams

Name of the Exam	Quantitative	Equally Weighted	Verbal

****** ALES: Akademik Personel ve Lisansüstü Eğitimi Giriş Sınavı

Computer Skills

Program	Ability to Use